CHAPTER 3: TESTING & RESULTS

3.1 Introduction

This chapter presents the test methodology and the test results for the five control decked bulb T beams and the bridge model. The results are presented in the form of charts showing the relationship between the applied load and the response of the test specimens including deflection, strain of concrete, and strain in CFCC strands. In addition, for each test specimen, the ductility ratio was calculated to evaluate the failure mode analytically.

Four control beams were tested to failure under flexural loading, while one control beam was tested under shear loading to failure. The bridge model was exposed to several loading scenarios at the service limit state, post-cracking limit state, and strength limit state. While testing of the control beams was conducted to evaluate the flexural and shear response, testing of the bridge model was conducted to evaluate the integrity of the entire superstructure and the probability of developing longitudinal deck cracking especially with the absence of a cast-in-place deck slab.

3.2 Flexural testing of Beam C-S-F-U

Beam C-S-F-U had a total length of 41 ft and was constructed with four bottom prestressed CFCC strands in addition to five top non-prestressed CFCC strands, two web non-prestressed CFCC strands, and steel stirrups. The theoretical analysis for the cross section using force equilibrium and strain compatibility indicated a tension failure by rupture of CFCC prestressing strands. During the test, the beam was simply supported over two elastomeric bearing pads with an effective span of 40 ft. The bearing pads had a length of 12.0 in., a width of 6.0 in., and a thickness of 1.0 in. The load was applied to the beam using a steel spreader with two-point load as shown in Figure 3.2-1. The distance between the points of loading was 78 in. This distance was maintained through the testing of this control beam and other flexurally tested control beams.

The test was commenced by applying the load through load cycles. After every load cycle, the beam was inspected and marked for cracks. The load cycles were applied in increments of 2 kip until the first flexural crack was observed and in increments of 4 kip from cracking to failure. The deflection of the beam was recorded using two Linear Motion Transducers (LMTs) attached to the soffit of the beam as shown in Figure 3.2-2.

Figure 3.2-1 Typical four-point-loading test setup for control beams

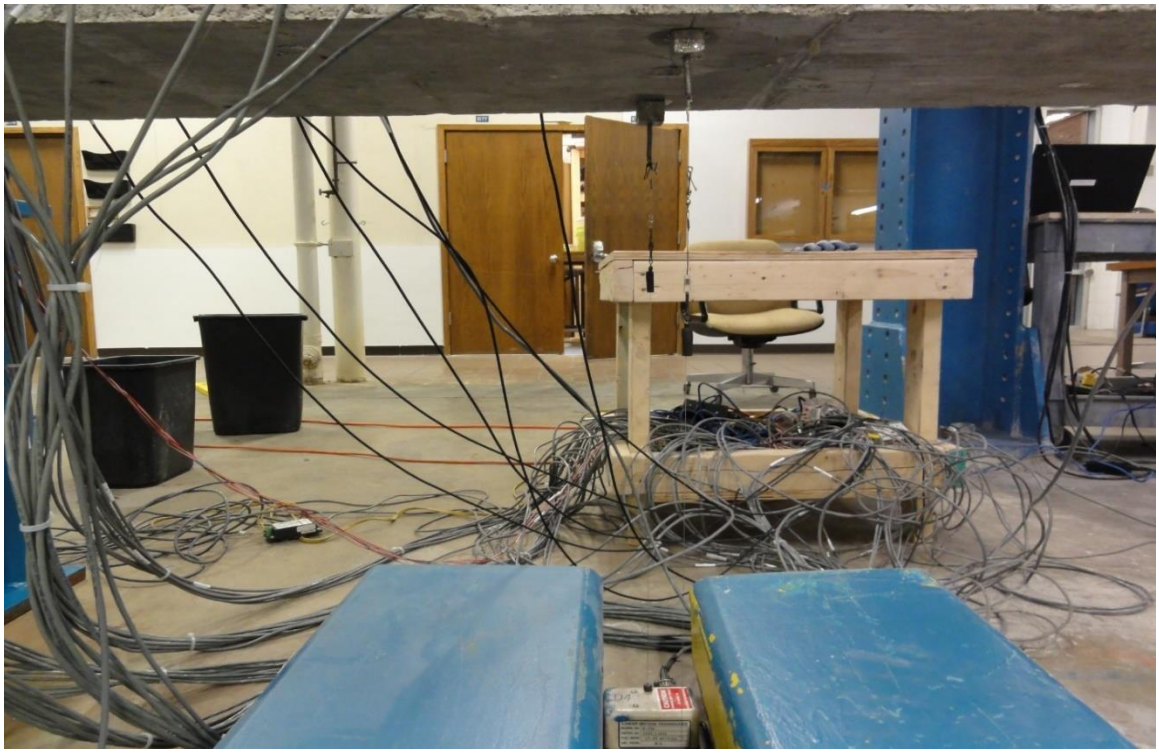

Figure 3.2-2 Linear motion transducers to evaluate deflection under different load levels

The first flexural crack was observed at a load level of 12.2 kip. This was confirmed from the recorded data as the load-deflection curves and the load-strain curves showed a remarkable change in the slope at nearly the same load level. After cracking, three strain gages were attached to the soffit of the beam near the first observed flexural crack and the load cycles were continued. The recoding from the three strain gages were used to estimate the average decompression load and consequently the average prestressing force in concrete after all losses. In subsequent load cycles, the applied load had to overcome the decompression in the beam due to prestressing before the flexural cracks can open again. Therefore, the strain gages around the crack provided strain readings until the decompression was overcome and the crack started to open. When the crack opened, the strain at the adjacent concrete ceased to increase and that marked the decompression load. The decompression load was also determined from the load deflection curves. In subsequent load cycles, an initial load was resisted by the pre-compressed section, which had the stiffness of a non-cracked gross section. Once the decompression load was reached, the stiffness dropped to that of a cracked section, and therefore, there was a remarkable change in the slope in the load-deflection curves at the decompression load in all post-cracking load cycles. The decompression load estimated using the readings from the soffit strain gages matched that estimated using the load-deflection curves and was approximately 9.9 kip, which represented a prestress loss of approximately 12 to 13 %.

The load cycles were continued and new cracks were marked after every load cycle as shown in Figure 3.2-3. The cracks were vertical and uniformly distributed under the loading spreader but they were inclined outside the loading points due to combined effect of shear and moment. As shown in Figure 3.2-4, this control beam was characterized with a dense crack map before failure. The cracks typically overlapped the stirrups and the average distance between the cracks was around 4 in., which matched the spacing between the stirrups. It should be also noted that the beam exhibited a significant deflection before failure. The deflection can be visually observed as shown in Figure 3.2-5. In practice, this deflection will be difficult to go unnoticed and it will be accompanied by cracking and collapse of non-structural components such as utility pipes, sidewalks, and barriers. Therefore, it serves as a significant visual warning sign before failure.

Figure 3.2-3 Crack mapping between load cycles

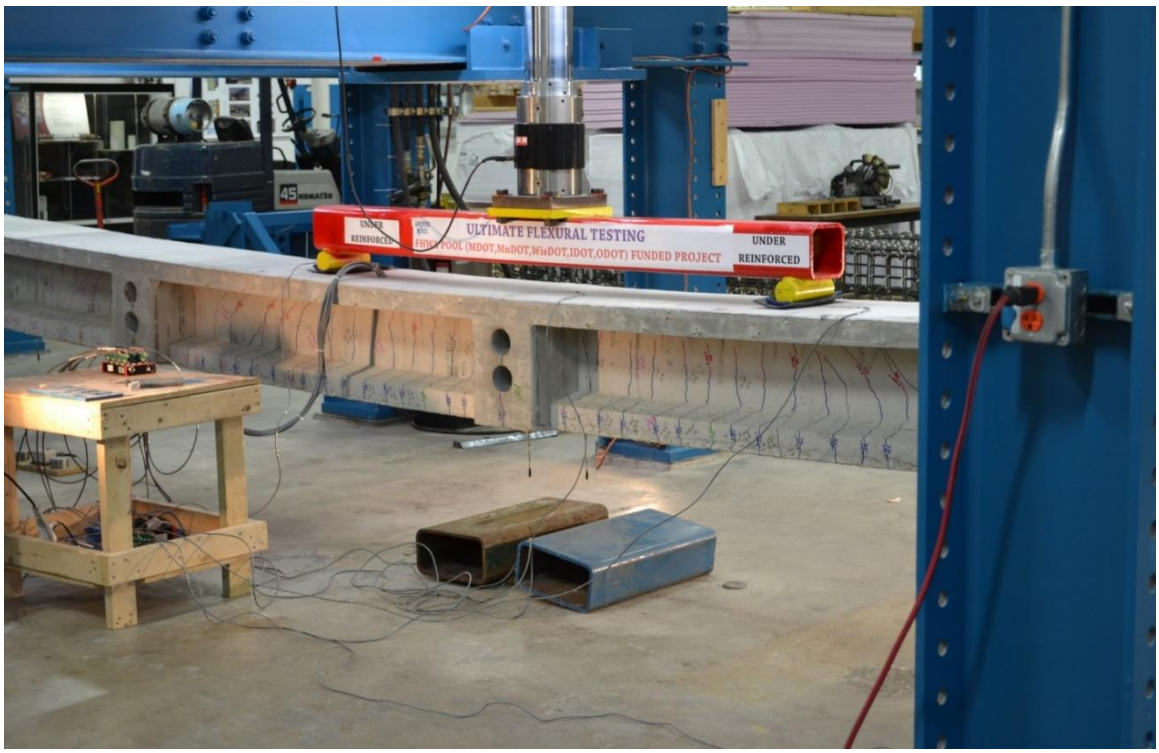

Figure 3.2-4 Load cycles of Beam C-S-F-U

Figure 3.2-5 Deflection of Beam C-S-F-U

The last load cycle before failure reached 24 kip with a corresponding deflection of 9.11 in. After unloading, the residual deflection from all load cycles was 0.82 in. as indicated in Figure 3.2-6. The last load cycle included loading the beam to failure. The failure of this control beam took place at a load level of 32.47 kip with a corresponding deflection of 14.42 in. (not including the residual deflection of 0.82 in.). At this load level, a popping sound was heard and the load slightly dropped to 31.72 kip with a corresponding deflection of 14.61 in. Then the beam continued to resist the load and the load level increased again to 33.19 kip with a corresponding deflection of 15.62 in. At that point, the popping sound was heard again and the load decreased to 31.55 kip with a corresponding deflection of 15.83 in. The beam however continued to take more load and approached a load level of 32.07 kip. Finally, multiple popping sounds were heard and the beam lost its structural integrity and sustained a permanent deformation as shown in Figure 3.2-7.

After failure, the beam was inspected and it was found that there was a spalling of the concrete cover at multiple locations (Figure 3.2-8). Failure in the CFCC strands was also observed and was linked to the concrete spalling (Figure 3.2-9). It was determined that the popping sounds that were heard during the test were the sound of CFCC strands rupture. However, it should be noted that

due to the configuration of the CFCC strand, which encompasses seven wires, the tensile failure usually occurs on the wire level and not the strand level. In other words, every popping sound heard could have represented the rupture of single wire in the CFCC strand.

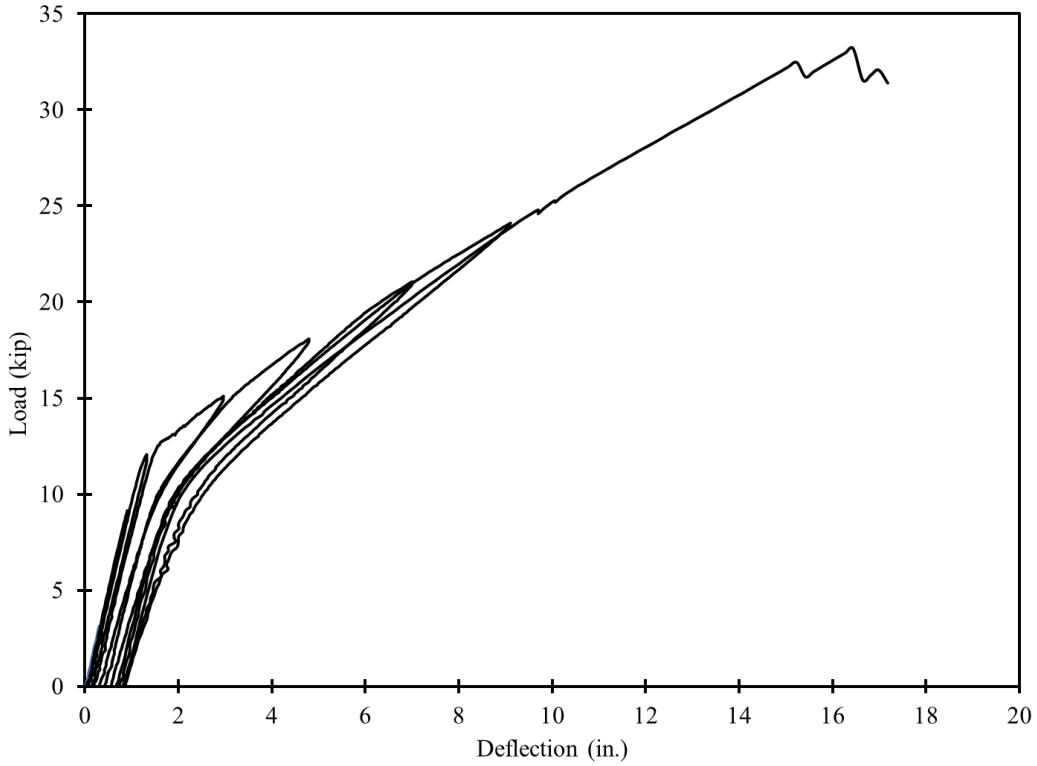

Figure 3.2-6 Load-deflection cycles of Beam C-S-F-U

Figure 3.2-10 and Figure 3.2-11 show the strain in the concrete top surface and the CFCC strands during the last load cycle. The maximum recorded concrete strain before failure was approximately 2,236 με, while the maximum recorded strain in the CFCC strands before failure was 18,233 με. The guaranteed ultimate strain in the CFCC as given by the manufacturer is 16,000 με. Therefore, it was evident that the failure took place in the CFCC strands (tension failure).

Finally based on the load-deflection curves from all load cycles including the ultimate load cycle, the ductility ratio was calculated according to Grace et al. (2000). The area under the load-deflection curve is divided into two areas of elastic and inelastic energies. The elastic energy is the energy that can be retrieved once the load is removed from the beam, while the inelastic energy is the energy dissipated in the formation of cracks and for high concrete strain, the energy dissipated by the plastic deformation of concrete. According to Figure 3.2-12, the total energy absorbed by beam C-S-F-U at failure was approximately 387 kip.in. By following the last un-loading curve and

estimate the un-loading curve at failure, the total energy was divided into elastic energy of 259 kip.in. and inelastic energy of 128 kip.in. The ductility ratio was calculated as the ratio between the inelastic energy and the total energy and was estimated as 33%. It should be noted that the mode of failure slightly increased the ductility ratio.

As expected, the ductility ratio of the beam indicated a brittle failure (ductility ratio less than 70%, Grace et al. (2000)). However, the large deflection and the dense cracking patterns give a clear visual sign before failure. The failure mode by the consecutive rupture in the individual wires of the strands may also be regarded as a warning sign before complete failure.

Figure 3.2-7 Beam C-S-F-U at failure

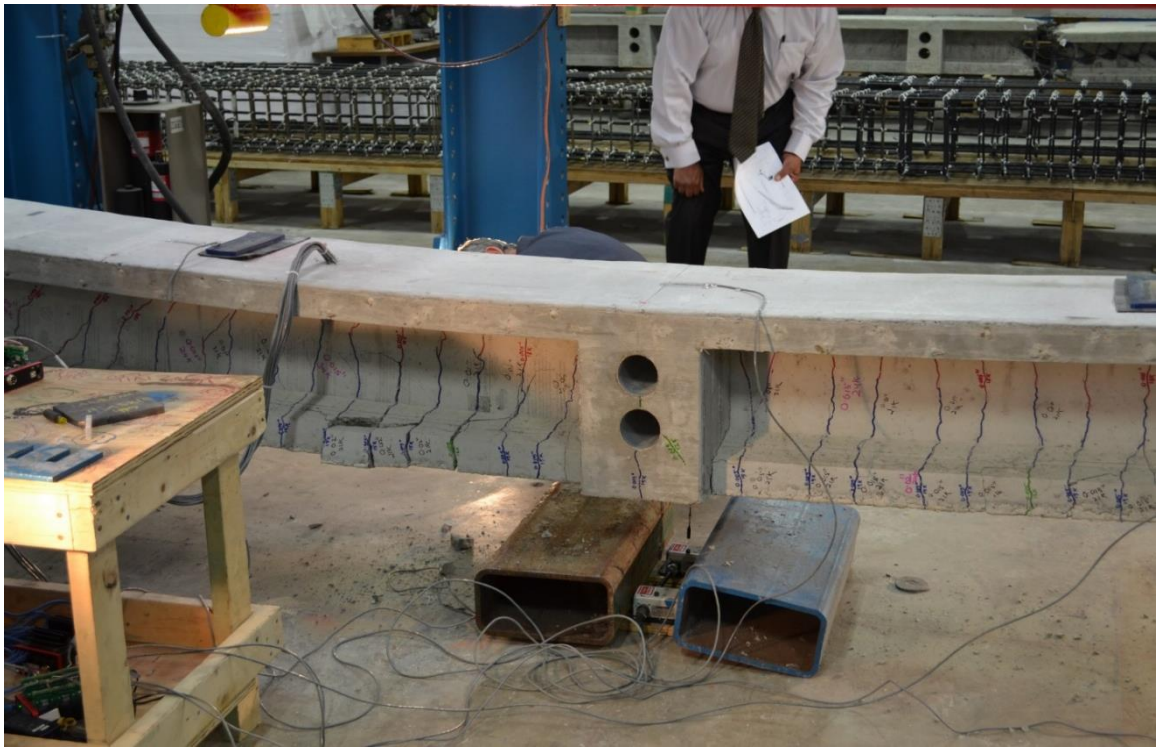

Figure 3.2-8 Spalling of concrete at failure in Beam C-S-F-U

Figure 3.2-9 Rupture of prestressing CFCC strands in Beam C-S-F-U

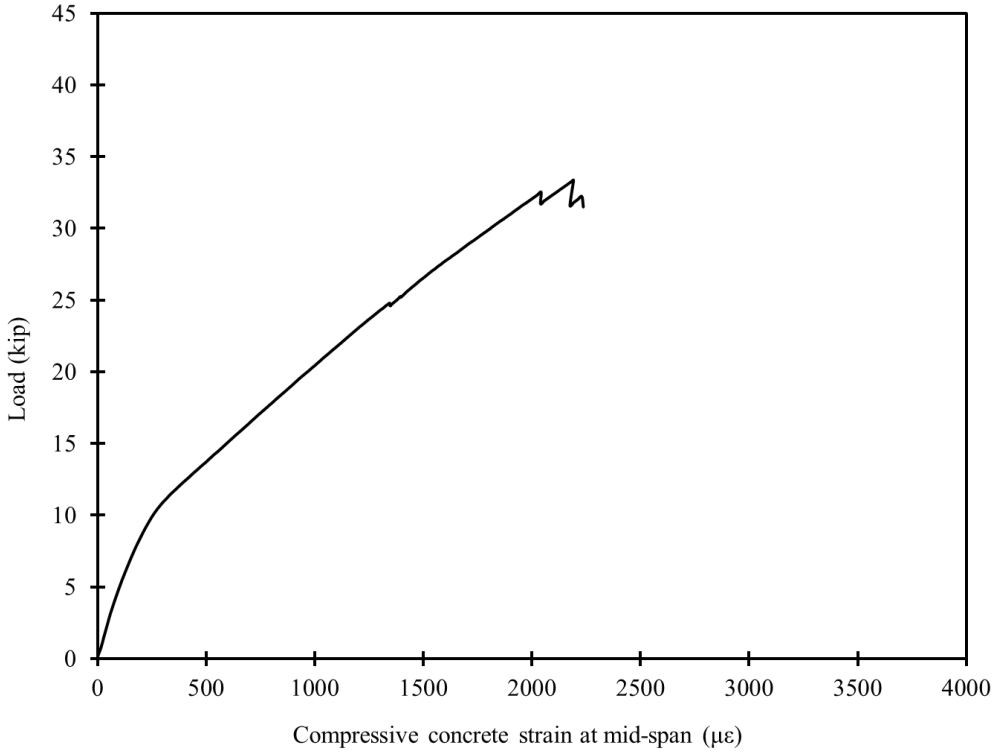

Figure 3.2-10 Load vs. concrete strain during last load cycle of Beam C-S-F-U

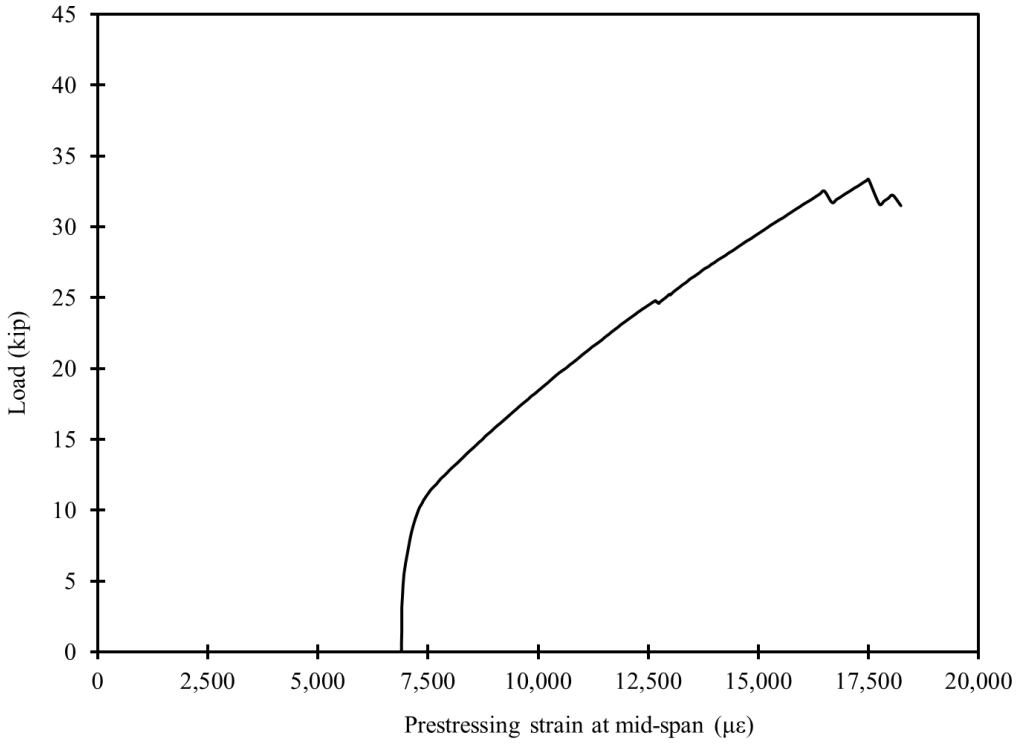

Figure 3.2-11 Load vs. strain of prestressing strands during last load cycle in Beam C-S-F-U

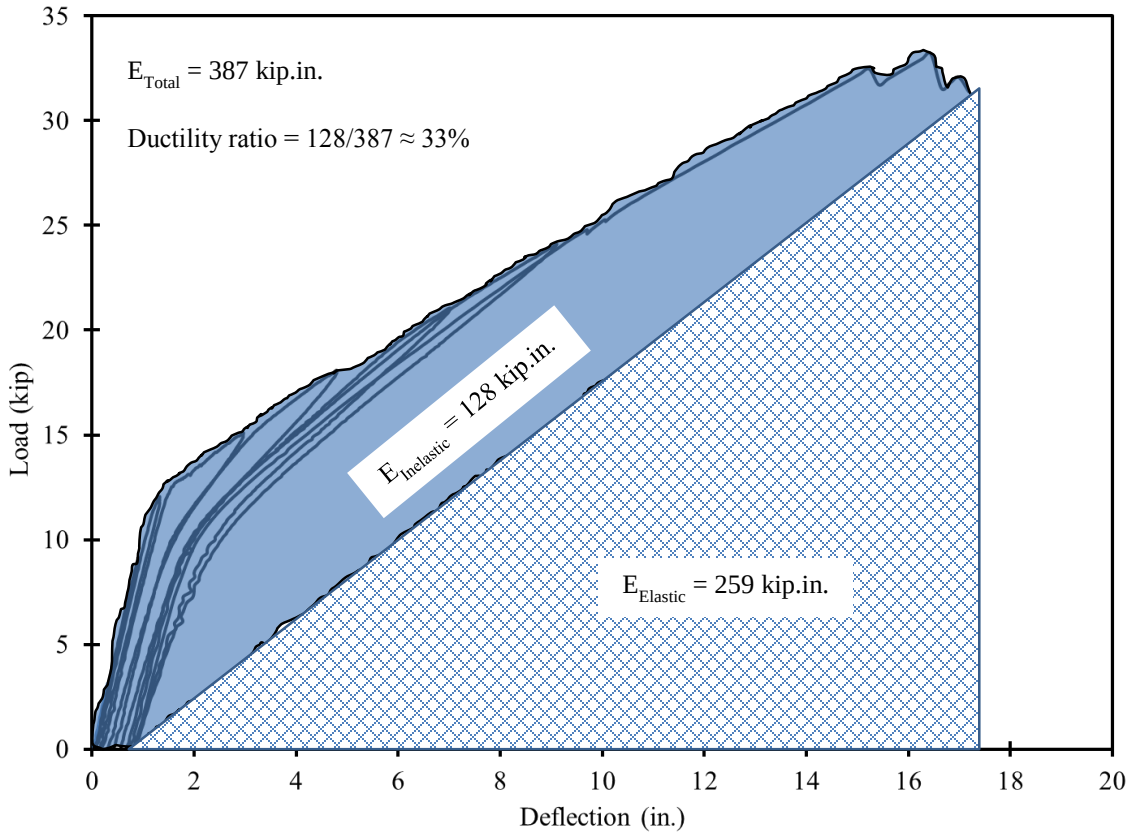

Figure 3.2-12 Ductility ratio in Beam C-S-F-U

3.3 Flexural testing of Beam C-S-F-B

This control beam was reinforced with four bottom CFCC prestressing strands and three bottom CFCC non-prestressing strands in addition to the top and web reinforcement. The beam was loaded under four-point flexural loading and the load was applied in cycles with a load increment of 2 kip before cracking and 4 kip after cracking. The last load cycle involved loading the beam to failure and as shown in Figure 3.3-1 and Figure 3.3-2, the failure resulted in breaking and total separation of the beam. The failure took place under one of the loading points, which represented the location of the maximum moment and maximum shear in the beam.

Similar to beam C-S-F-U, the observed cracking load was approximately 12 kip and the decompression load was estimated from strain readings and load-deflection curves as 9.5 kip. As shown in Figure 3.3-3, the last load cycle before failure reached 24 kip with a corresponding deflection of 8.24 in. After unloading, the remaining deflection from all load cycles was

approximately 0.95 in. The load cycles before cracking were characterized by a mono-slope load-deflection curves, while load cycles after cracking were characterized by a bilinear load-deflection curve. The decompression load marked the change of slope in all load-deflection curves performed after cracking.

The failure took place at a load level of 40.79 kip with a corresponding deflection of 16.98 in. or 17.94 in. after adding the residual deflection from previous load cycles. The concrete strain at failure reached 3,272 με. The strain in the concrete matched the theoretical analysis and indicated a balanced failure. Due to strain gages malfunctioning, the recording of the strain in prestressing strands was interrupted early at the test.

The total energy stored in the beam before failure (area under load-deflection curve) was approximately 447 kip.in. as shown in Figure 3.3-4. The elastic and inelastic energies were estimated (graphically and analytically) as 321 and 126 kip.in., respectively. The ductility ratio for this beam was estimated as 28%.

Figure 3.3-1 Balanced failure of Beam C-S-F-B

Figure 3.3-2 Balanced failure resulting in complete separation of Beam C-C-F-B

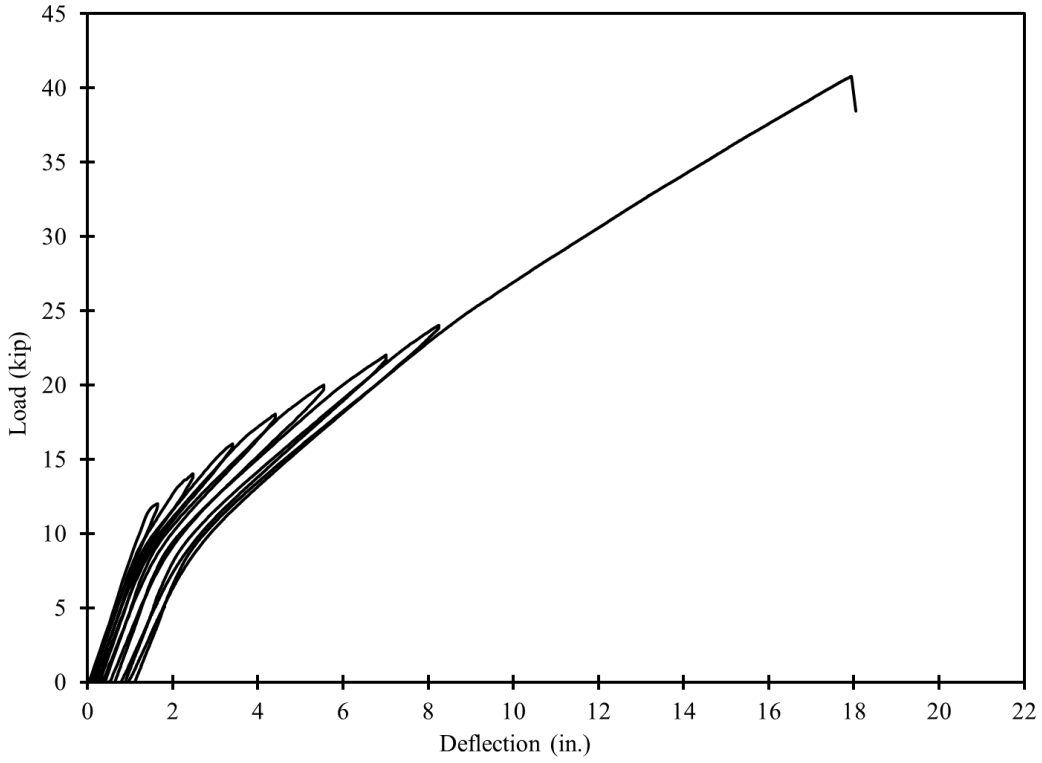

Figure 3.3-3 Load-deflection curves for Beam C-S-F-B

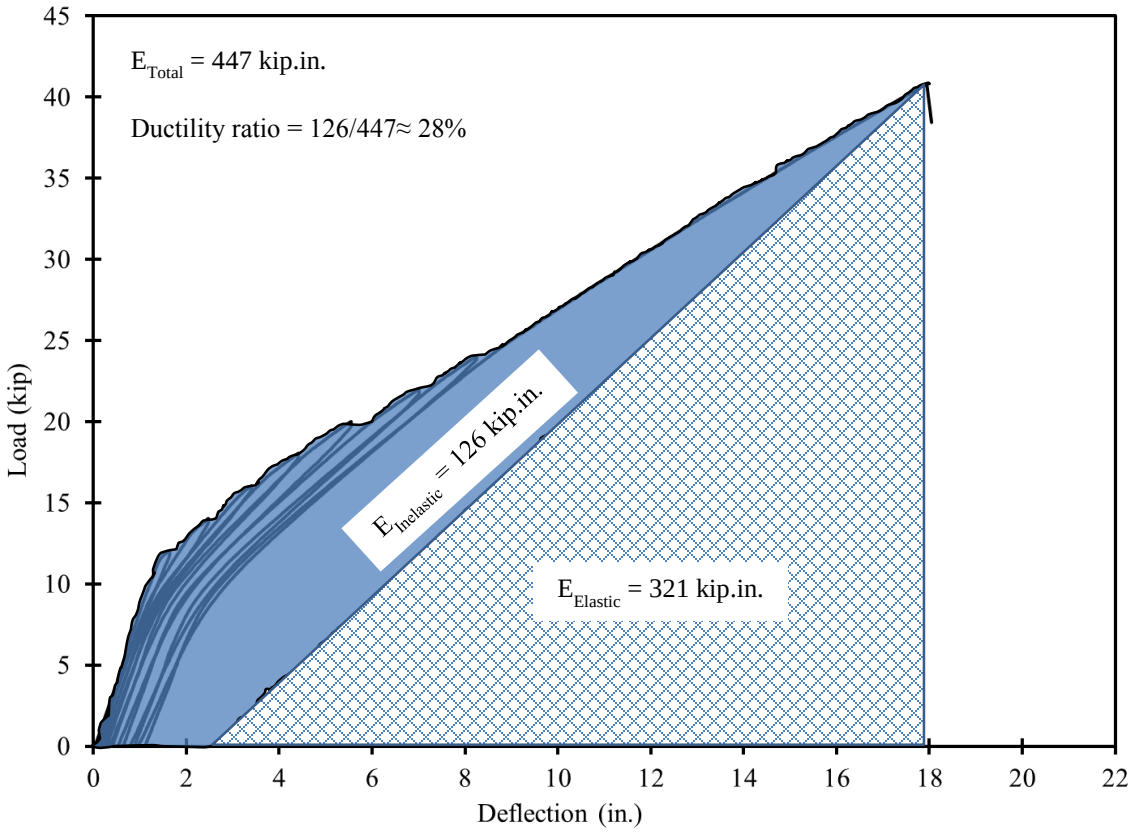

Figure 3.3-4 Ductility ratio in Beam C-S-F-B

3.4 Flexural testing of Beam C-S-F-O

This control beam was provided with four bottom prestressing CFCC strands and five bottom non-prestressing CFCC strands. This amount of bottom reinforcement guaranteed the compression failure mode. As shown in Figure 3.4-1 through Figure 3.4-3, the failure of this beam was characterized by the crushing of the concrete in the top flange followed by shearing and rupturing of both prestressing and non-prestressing CFCC strands and breaking of the beam into two pieces.

The failure of the beam took place at a load level of 43.6 kip with a corresponding deflection of 14.89 in. or 15.59 in. with the added residual deflection from previous load cycles. The maximum recorded concrete strain in the top flange before failure was approximately 2,951 με, while the maximum recorded strain in the prestressing strands at failure was approximately 13,665 με.

Figure 3.4-4 shows the load-deflection curves obtained from all load cycles. Similar to previous beams, mono-slope linear curves were obtained before cracking, while bilinear curves

were obtained after cracking with the decompression load marking the change in slope. The cracking load was around 12.3 kip, while the decompression load was estimated as 9.5 kip. The last load cycle before failure reached 34 kip with a corresponding deflection of 11.01 in. After unloading, the residual deflection from all load cycles was approximately 0.7 in.

Figure 3.4-5 highlights the elastic and inelastic energy absorbed by the beam before failure. The elastic energy was approximately 280 kip.in., while the inelastic energy was approximately 123 kip.in. with a total energy of 403 kip.in. and a ductility ratio of 31%. Similar to previous beams with CFCC reinforcement, from the aspect of ductility ratio, the failure of the beam falls under the brittle failure category but from a deflection and cracking perspective, the failure was accompanied by enough warning signs that indicated the overstressing.

Figure 3.4-1 Beam C-S-F-O at failure

Figure 3.4-2 Compression failure followed by rupture of strands in Beam C-S-F-O

Figure 3.4-3 Close view showing the failure section of Beam C-S-F-O

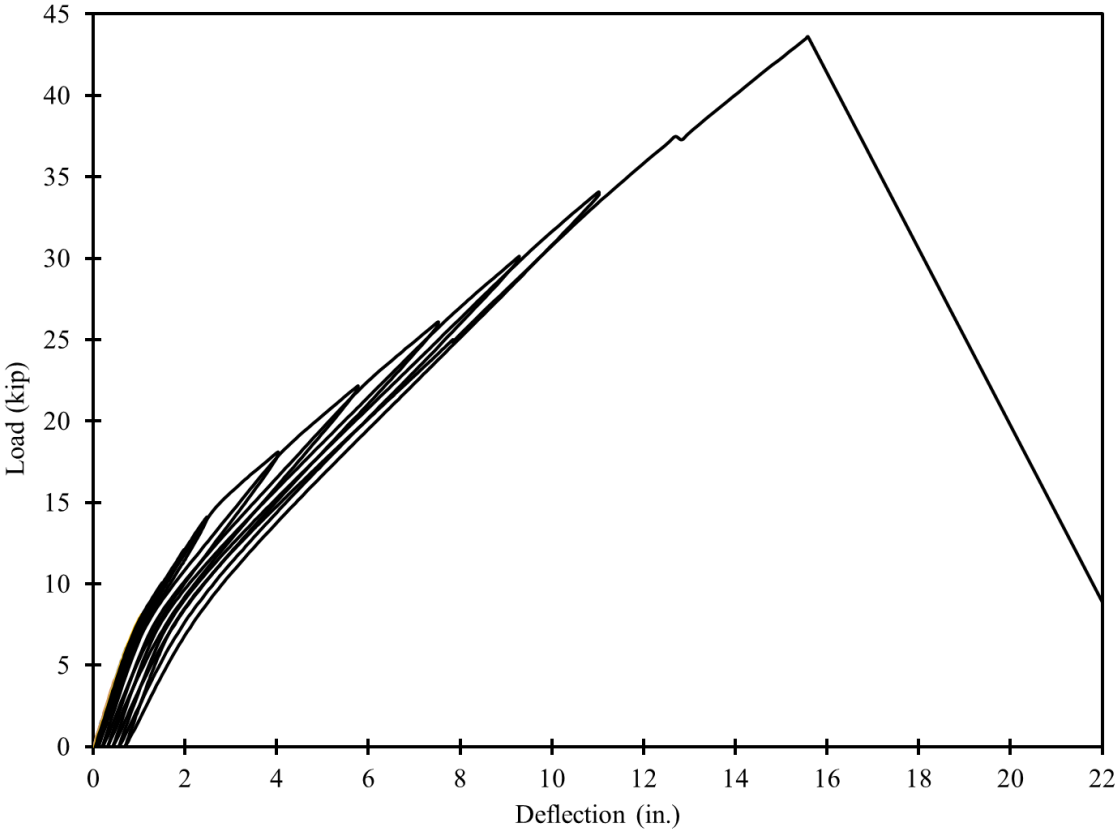

Figure 3.4-4 Load-deflection curves for Beam C-S-F-O

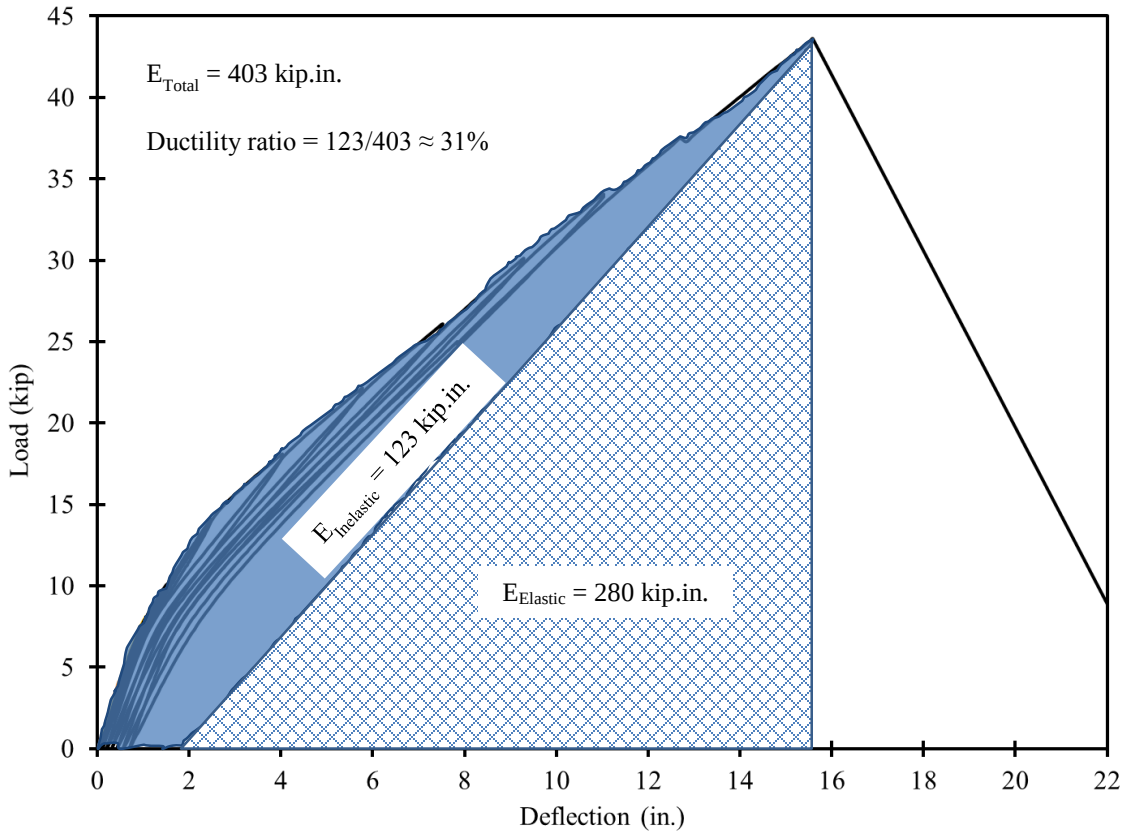

Figure 3.4-5 Ductility ratio of Beam C-S-F-O

3.5 Flexural testing of Beam S-S-F-U

This beam was prestressed with four bottom low-relaxation steel prestressing strands in addition to three non-prestressed deformed steel bars. The configuration of reinforcement was similar to that of the balanced CFCC beam, Beam C-S-F-B. However, because of the difference in material properties between steel and CFCC, this beam was expected to fail in tension by yielding of prestressing strands. Similar to other control beams, this beam was tested under four-point loading applied through cycles of loading and unloading. The cracking load and the decompression load were around 12 kip and 9.5 kip, respectively. The last load cycle before failure reached 30 kip with corresponding deflection of 7.03 in. After unloading, the residual deflection was approximately 0.74 in.

During the last load cycle, the beam exhibited yielding of strands at a load level of 30.6 kip with a corresponding deflection of 7.52 in. (including the residual deflection). After yield, the deflection of the beam increased successively with a smaller increase in the applied load. The

failure took place at a load level of 39.37 kip with a corresponding deflection of 20.17 in. (including the residual deflection). At failure, the concrete in the top flange crushed and the top reinforcement showed signs of buckling as shown in Figure 3.5-1 through Figure 3.5-3. The maximum recorded concrete strain before failure averaged 2,615 με, while the strain in the prestressing steel strands averaged 18,784 με. From the results and as shown in Figure 3.5-4, it can be seen that approximately 12.65 in. of deflection was obtained between steel yield and concrete crushing with a corresponding load increase of approximately 8.77 kip.

Due to the yielding of prestressing strands, this control beam exhibited a high ductility ratio. As shown in Figure 3.5-5, the total energy absorbed before failure was estimated as 613 kip.in. The elastic energy was estimated as 185 kip.in, while the inelastic energy was estimated as 428 kip.in. Therefore, the ductility ratio was calculated as 70%, which places this failure within the ductile failure boundaries.

Figure 3.5-1 Flexural failure of Beam S-S-F-U

Figure 3.5-2 Failure of Beam S-S-F-U showing crushing of concrete after yield

Figure 3.5-3 Buckling of top reinforcement in Beam S-S-F-U at failure

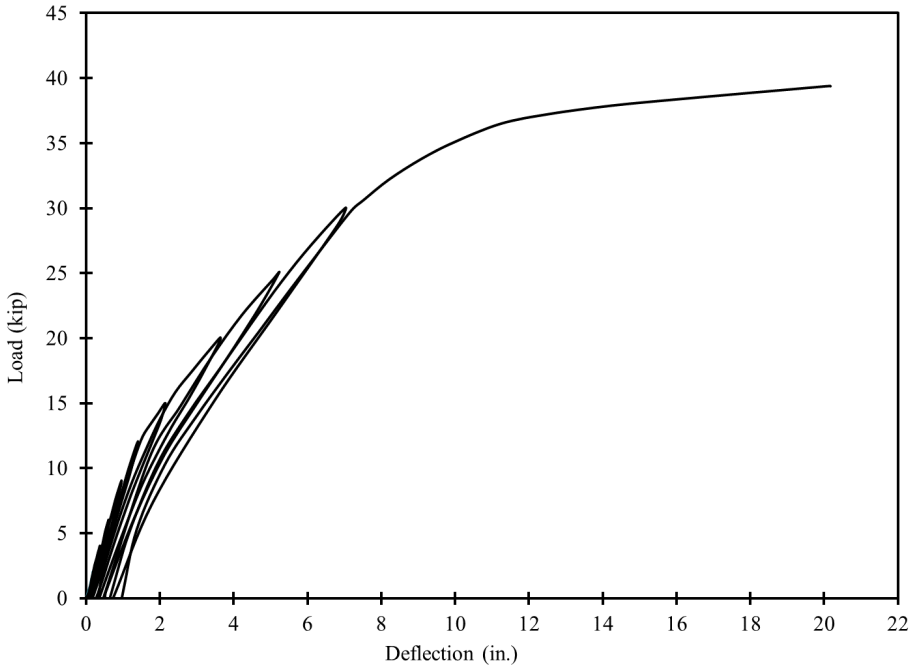

Figure 3.5-4 Load-deflection curves for Beam S-S-F-U

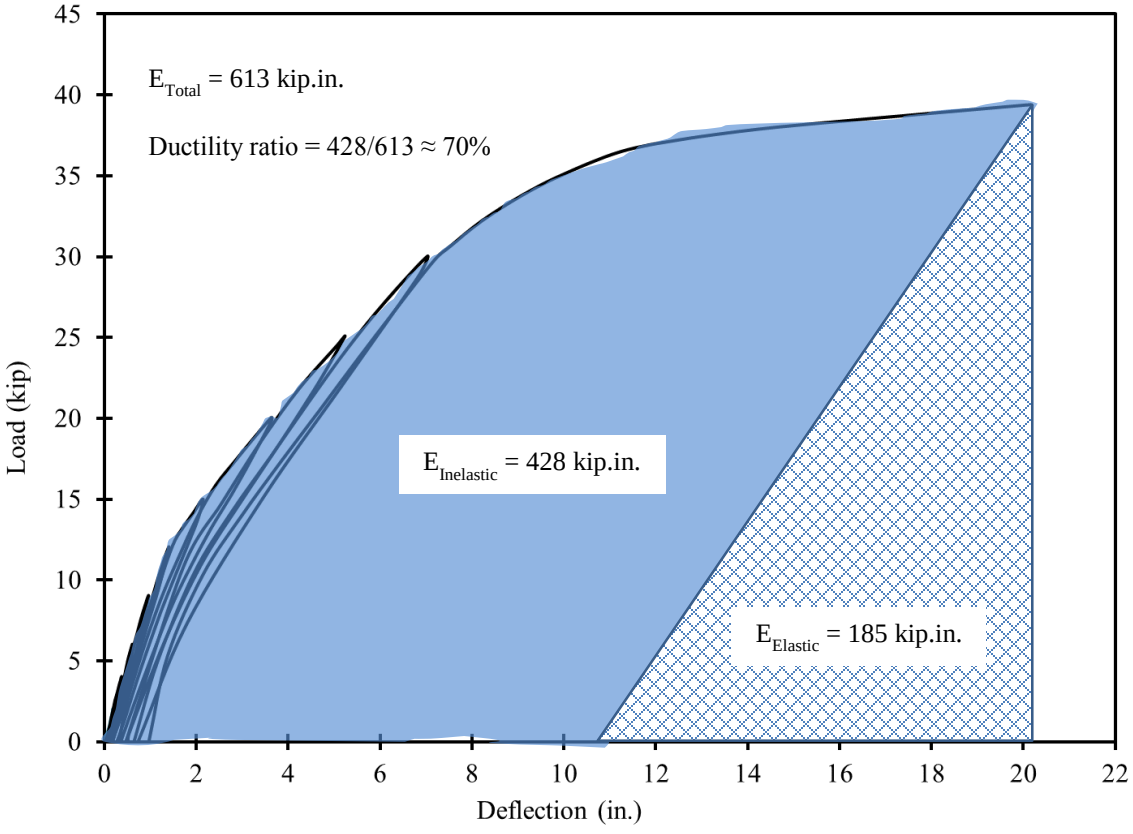

Figure 3.5-5 Ductility ratio in Beam S-S-F-U

3.6 Comparison between flexural control beams

The load-deflection curves during the ultimate-load cycle for all control beams are plotted in Figure 3.6-1 with elimination for the residual deflection from previous load cycles. All the beams had the same stiffness before reaching the decompression load. After the decompression load, Beam S-S-F-U with steel strands had the highest stiffness followed by Beam C-S-F-O, Beam C-S-F-B, and finally Beam C-S-F-U. The difference in bending stiffness between control beams with CFCC reinforcement was attributed to the difference in reinforcement ratio, while the difference in stiffness between Beam S-S-F-U and other control beams was attributed mainly to the difference in material properties between steel and CFCC.

The recorded concrete strain in all beams at the mid-span during the ultimate load cycle is shown in Figure 3.6-2. Strain readings in beam S-S-F-U were significantly less than those in other control beams until yielding. After yielding the concrete strain in beam S-S-F-U increased rapidly and approached those of beams C-S-F-B and C-S-F-O. It should be noted that the recorded strain does not necessarily represent the maximum strain in the concrete flange as it only represents the strain at the location of the gages. However, it can be seen that the concrete crushing in beams S-S-F-U, C-S-F-B, and C-S-F-O occurred at approximately 3000 $\mu\varepsilon \pm 400\ \mu\varepsilon$. Figure 3.6-3 shows the average strain readings in the prestressing strands in all control beams during the last load cycle. As mentioned earlier, the prestressing strain recoding in Beam C-S-F-B was interrupted and stopped early at the test. The ultimate load and maximum strain and deflection readings for all beams are presented in Table 3.6-1, which also shows the design factored load for each beam when including all strength reduction factors.

The design factored load was analytically calculated by estimating the theoretical nominal capacity of each beam and multiplying this nominal capacity by the appropriate strength reduction factor according to available design guides. A strength reduction factor of 0.65 (ACI 440.4R-04) was included in case of CFCC prestressed beam with compression failure and a strength reduction factor of 0.85 was implemented in case CFCC prestressed beam with tension failure. Beam S-S-F-U with prestressing steel strands was designed with a strength reduction factor of 1.0 (AASHTO LRFD 2012). In addition, a CFCC guaranteed strength of 339 ksi was used in the design and it was further reduced to 304.9 ksi to account for the exposure to environmental conditions (ACI 440.1R-06).

Table 3.6-1 Summary for the ultimate-load testing of control beams

Beam	Crack/ service load (kip)	Decomp. load (kip)	Ultimate load (kip)	Defl. at failure (in.)	Concrete strain at failure (με)	Prestress strain at failure (με)	Design factored load (kip)
C-S-F-U Under-Reinf. CFCC	12.2	9.9	33.19	15.62	2,236	18,233	23.0
C-S-F-B Balanced CFCC	12.0	9.5	40.79	17.00	3,272	-	28.1
C-S-F-O Over-Reinf. CFCC	12.3	9.5	43.6	14.89	2,951	13,665	30.5
S-S-F-U Under-Reinf. steel	12.0	9.5	39.37	19.43	2,615	18,787	34.6

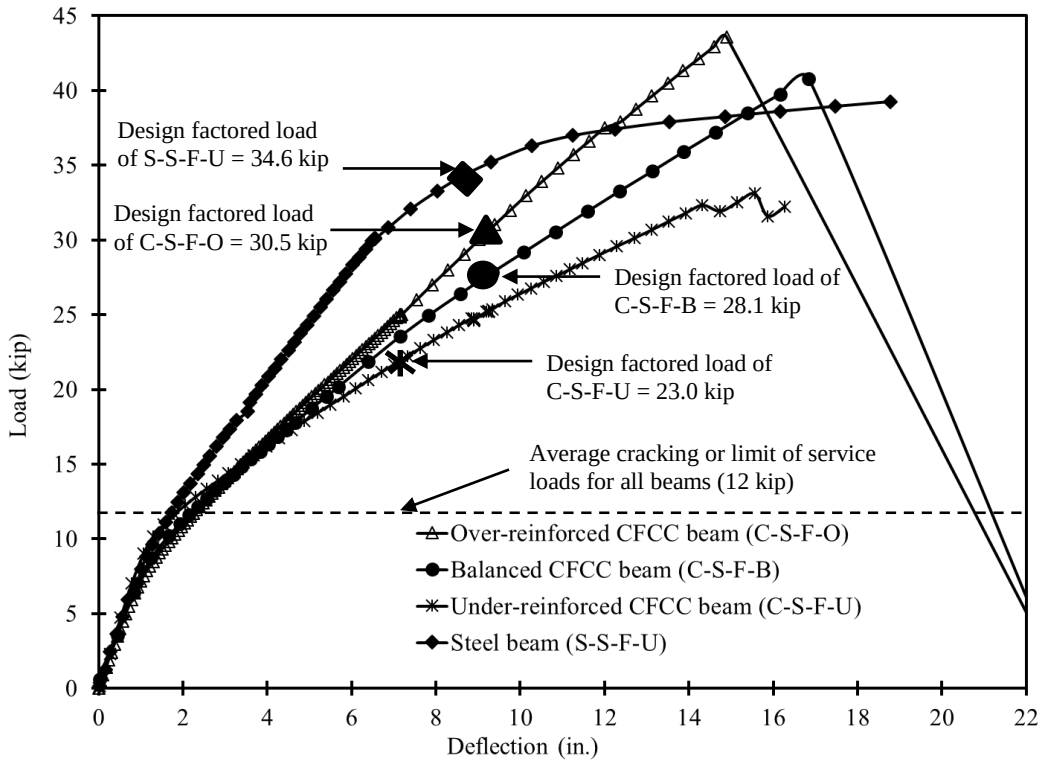

Figure 3.6-1 Load-deflection curves for all control beams tested in flexure

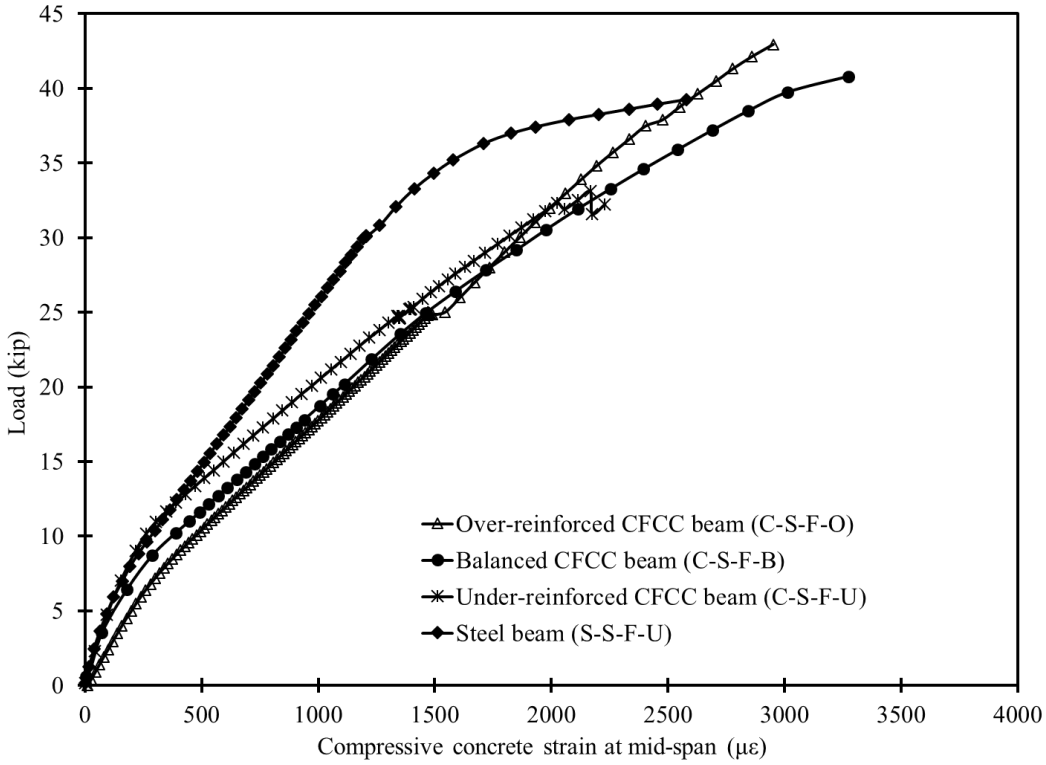

Figure 3.6-2 Load-concrete-strain curves for all control beams tested in flexure

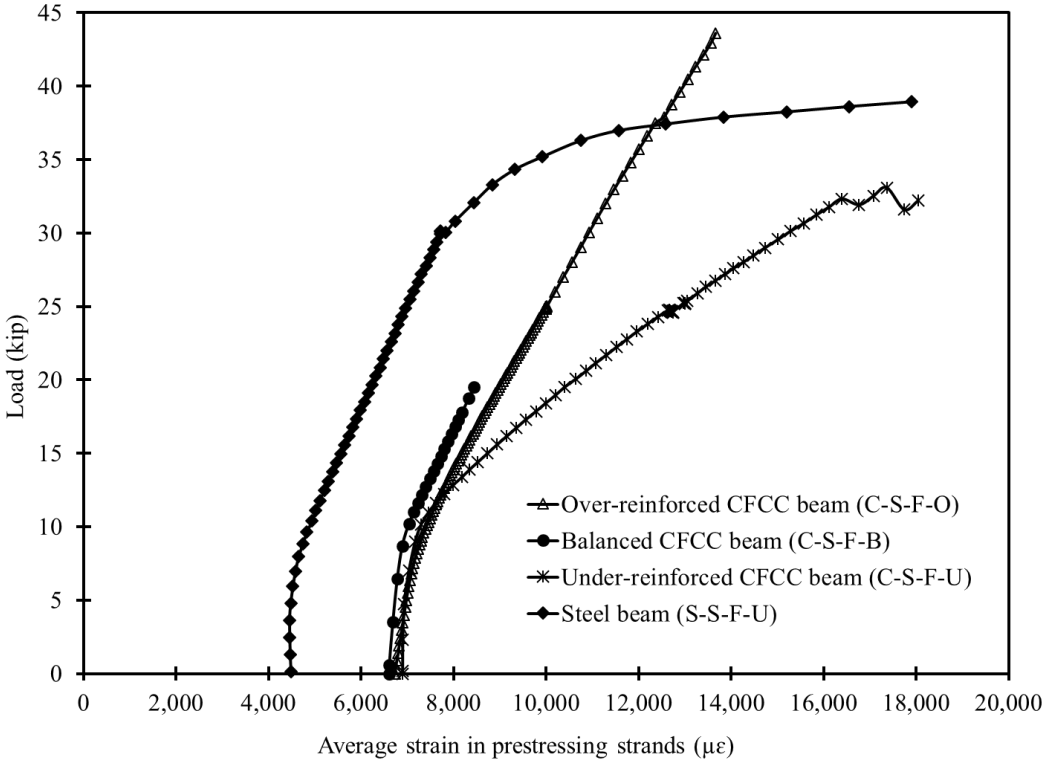

Figure 3.6-3 Load-prestressing-strain curves for control beams tested in flexure

3.7 Shear testing of Beam C-C-S-B

This control beam was reinforced with four bottom prestressing CFCC strands and three non-prestressing CFCC strands. In the transverse direction, the beam was provided with CFCC stirrups at a center-to-center spacing of 4.0 in. The beam had a total length of 41 ft and effective span of 40 ft and was simply supported over two elastomeric bearing pads.

In shear testing, the shear loading mechanism is affected by the distance from the applied load to the nearest support, or the shear span distance. If the shear span distance is very small, the load is typically transferred to the support through arch action and the shear reinforcement does not participate in the shear load carrying mechanism. If the shear span is long, the failure is usually a combination between the shear and flexural failure. Previous studies (Tuchscherer et al. 2011 and Zsutty 1971), uses the shear-span-to-depth ratio as a means of evaluating the failure mode. For instance, it was observed that arch action failure is the dominant failure mode in beams with shear-span-to-depth ratio less than 2.5, while shear failure dominate beams with shear-span-to-depth ratios ranging between 2.5 to 6.0, and flexural failure dominates beams with shear-span-to-depth ratios larger than 6.0.

As shown in Figure 3.7-1, the load was applied near the end of the beam with an effective shear span of 45 in., which resulted in a shear-span-to-depth ratio of 3.0 and consequently promoted the shear failure in this control beam. To capture the shear loading mechanism and the shear failure mode, the beam was instrumented with multiple LVDTs to record the slippage of CFCC strands at the end of the beam as shown in Figure 3.7-2. The beam was also provided with a series of linear strain gages, rosette strain gages, and LVDTs through the shear span as shown in Figure 3.7-3 and Figure 3.7-4. In addition, strain gages were provided on the top flange near the loading point to record the strain in the concrete. LMTs were attached to the beam under the point of loading and under the mid-span section.

Internally, each stirrup through the shear span was provided with two strain gages as shown in Figure 3.7-5. The stirrups were labeled from S1 near the support to S8 just under the load. In addition, all the internal reinforcement including the prestressing CFCC strands was provided with strain gages at the section under load.

The testing of the beam started with applying the load in cycles of loading and unloading. After each loading cycles, the beam was inspected for cracks. The first observed crack was a shear crack that developed through the web of the beam. The readings from the rosette strain gages confirmed the developed crack as the cracking stress of the web was exceeded at the development of the first shear crack at a shear force level of 25.64 kip. The shear force is equal to the reaction at the near support. After cracking, the readings from the strain gages did not represent the exact stress and strain distribution at the shear span and therefore was not presented here to avoid confusion. However, these readings were analyzed to evaluate the compression stress in the concrete struts between shear cracks. Figure 3.7-6 and Figure 3.7-7 show the development of the shear cracks during different loading stages until just before failure.

On the other side of the beam, the LVDTs recorded significant relative displacements only after cracking. As the LVDTs crossed the shear cracks, the average crack width was determined by analyzing the readings from the LVDTs in three different directions 0, 45, and 90 degrees according to Shehata (2000).

With increasing the load, the existing shear cracks propagated and new shear cracks developed. In addition, some shear cracks developed into flexural cracks. The first flexural crack was observed at a shear force level of 41 kip.

The failure of the beam took place at a shear force level of 41.24 kip. The failure was explosive in nature (Figure 3.7-8). The only warning sign was the development of a main diagonal shear crack extending from the support after the diaphragm and across the shear span to the loading point. The failure was characterized by the crushing of the concrete strut in the web and subsequently in the deck flange as shown in Figure 3.7-9. After failure, the stirrups were exposed and inspected for failure but no rupture of CFCC stirrups was observed (Figure 3.7-10).

As shown in Figure 3.7-11, the maximum recorded compressive concrete strain in the top flange under the load was approximately 2,668 με, while the maximum record strain in the web at 45° was approximately 1,935 με. On the other hand, the maximum deflection under load and at mid-span at failure was approximately 3.29 in. and 5.71 in., respectively. As shown in Figure 3.7-12, both deflection curves under load and at mid-span were bilinear curves with the decompression load marking the change of the slope between the two linear segments of each curve.

Figure 3.7-13 shows the strain in selected stirrups during the ultimate load cycles. It should be noted that during initial load cycles, the strain in the stirrups was negligible until the development of first flexural crack. On crack development, stirrups intercepted by the crack showed a sudden increase in the strain, while stirrups not intercepted by cracks did not show any significant strain reading. The readings shown in Figure 3.7-13 represent the maximum recorded strain in stirrups as those stirrups were intercepted by shear cracks in previous load cycles. The maximum recorded strain in the stirrups at failure was that recorded by the bottom strain gage in S3 and was approximately 3,720 με. By looking at Figure 3.7-5, it can be seen that there was a major shear crack crossing near that particular strain gage and that shear crack developed to be the failure plane as shown in Figure 3.7-8 and Figure 3.7-9. Finally, Figure 3.7-14 shows the average shear crack width as calculated based on the readings from the LVDTs. The maximum recorded shear crack width was approximately 0.09 in. It should be noted that the maximum limit of the LVDTs was exceeded near failure and that was the reason for the constant crack width reading near the failure.

Figure 3.7-1 Test setup of Beam C-C-S-B

Figure 3.7-2 Monitoring slippage of prestressing CFCC strands using end LVDTs

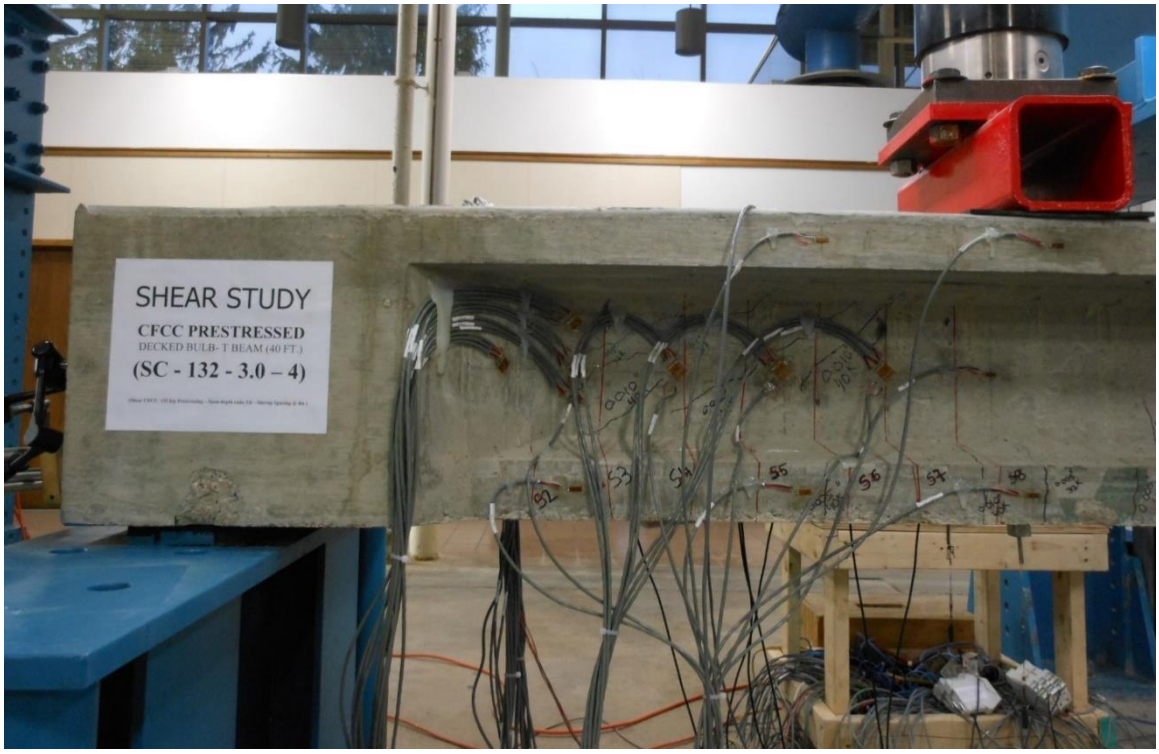

Figure 3.7-3 Strain gages through shear span of Beam C-C-S-B

Figure 3.7-4 LVDTs at 0, 45, and 90° to evaluate shear cracking

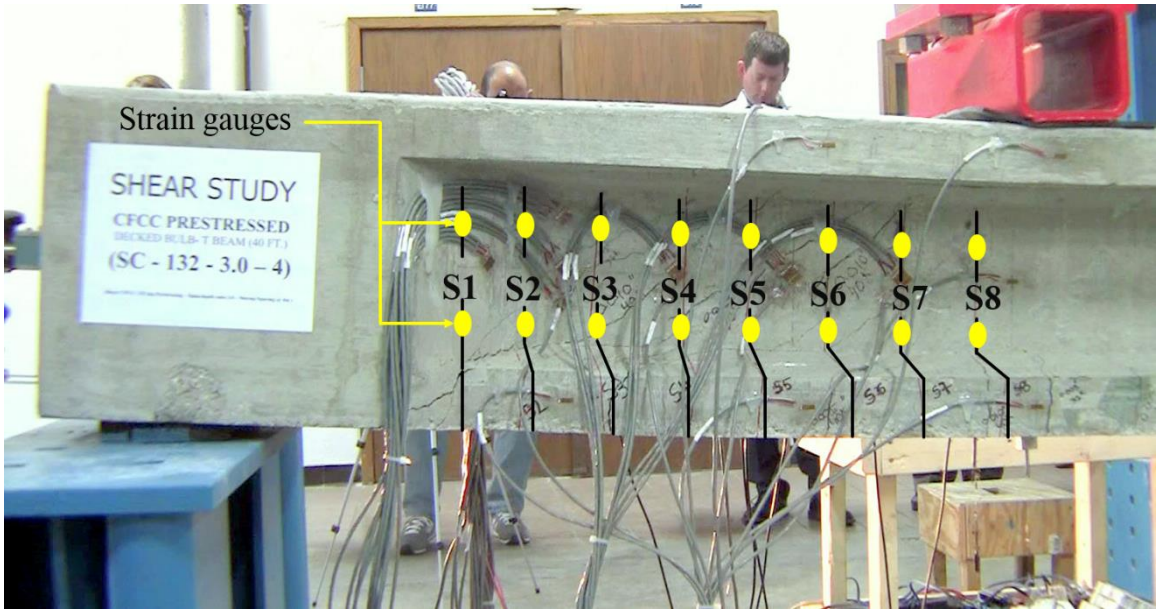

Figure 3.7-5 Location of internal strain gages on CFCC stirrups of Beam C-C-S-B

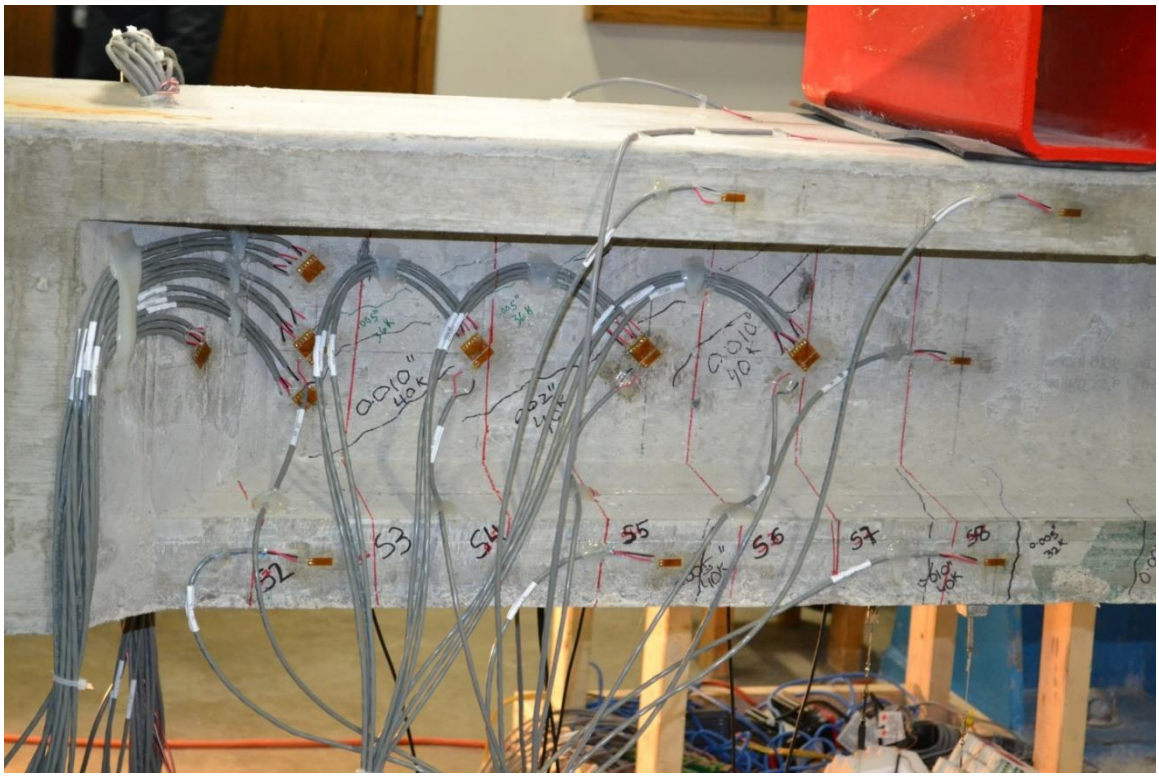

Figure 3.7-6 Crack development in shear span of Beam C-C-S-B

Figure 3.7-7 Development of main shear crack just before failure in Beam C-C-S-B

Figure 3.7-8 Explosive failure of Beam C-C-S-B

Figure 3.7-9 Beam C-C-S-B after failure

Figure 3.7-10 No rupture of CFCC stirrups was observed in Beam C-C-S-B

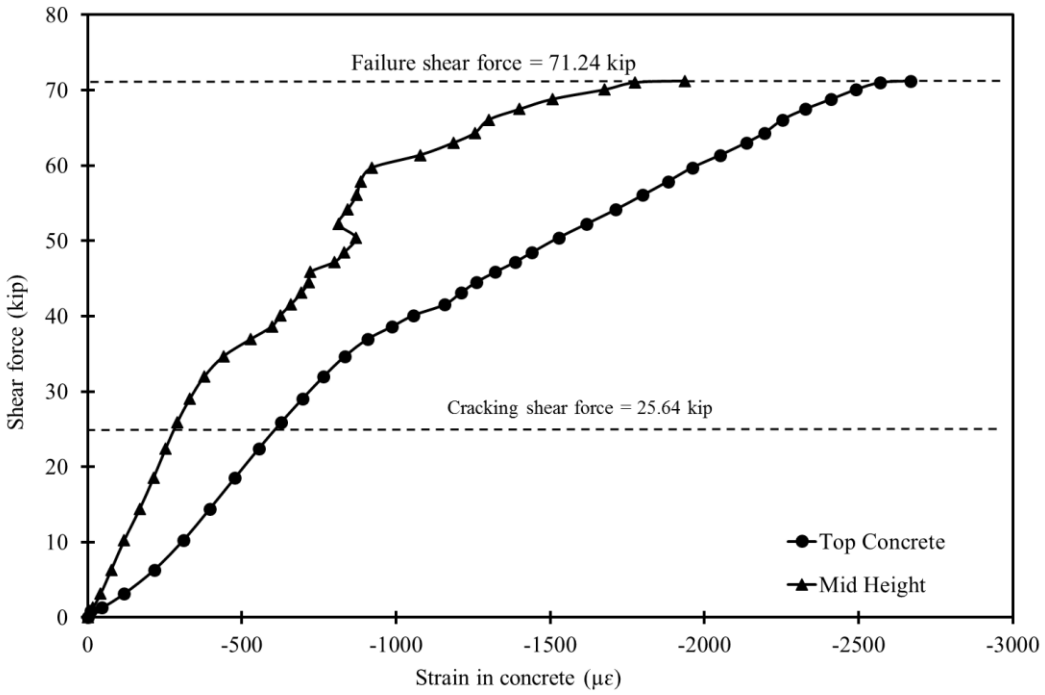

Figure 3.7-11 Recorded concrete strain under loading point of Beam C-C-S-B

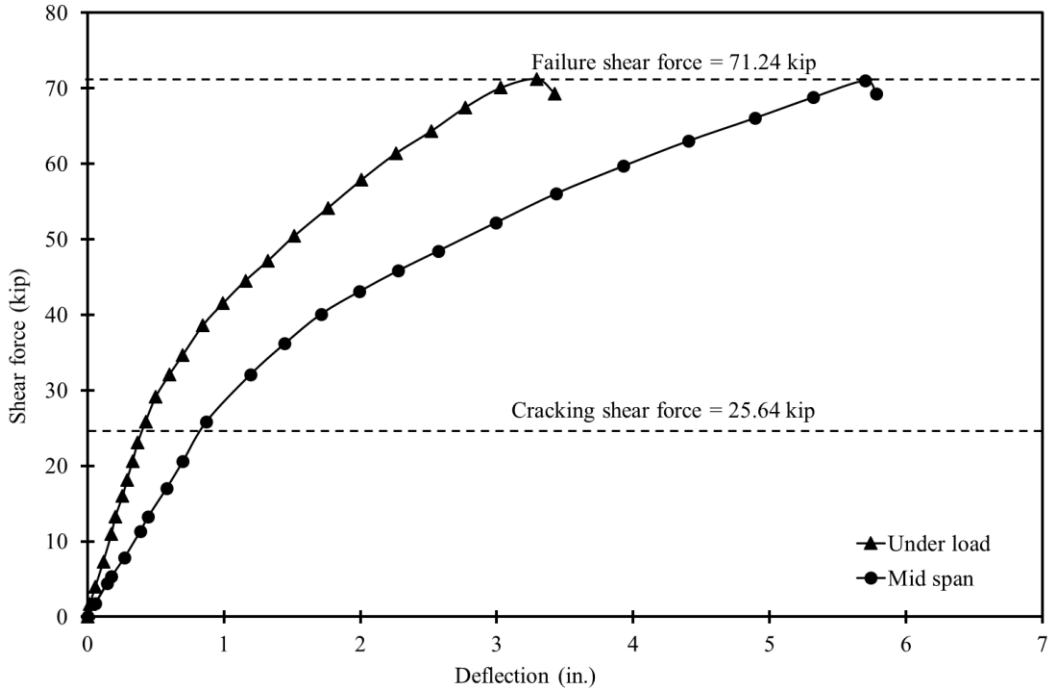

Figure 3.7-12 Recorded deflection under load and at mid-span of Beam C-C-S-B

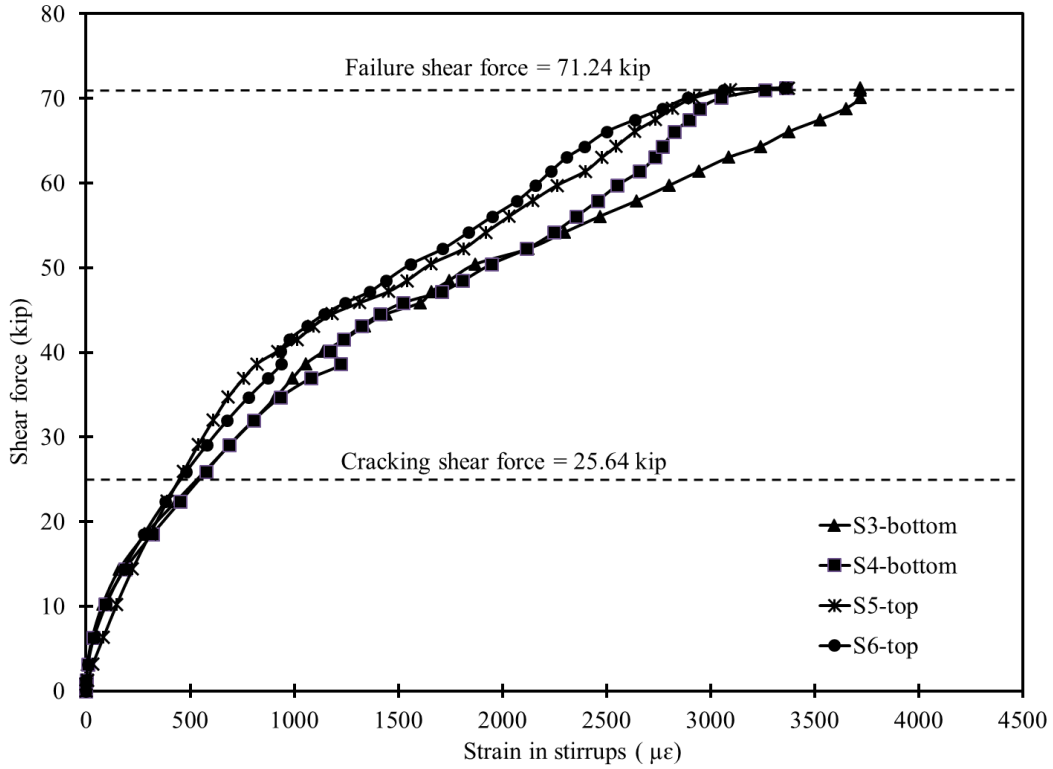

Figure 3.7-13 Shear force vs. stirrup strain in Beam C-C-S-B

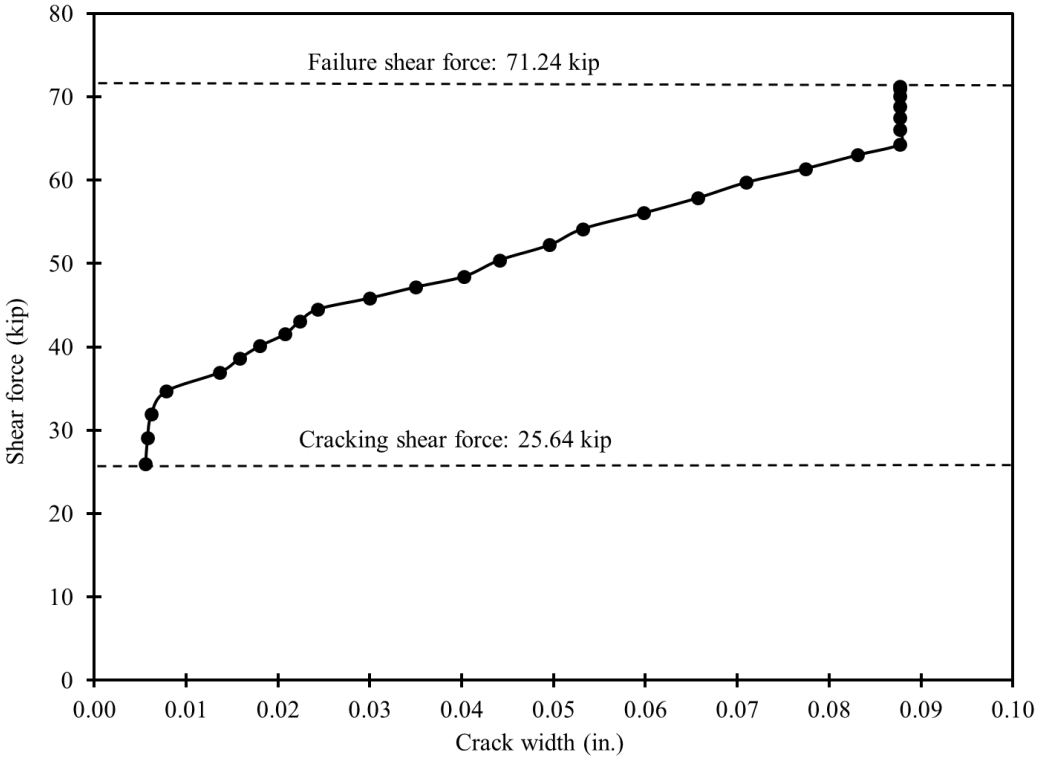

Figure 3.7-14 Shear force vs. calculated crack width in Beam C-C-S-B

3.8 Testing of bridge model

The bridge model was subjected to several testing scenarios. The first testing scenario included applying a service point load at the mid-span of each beam. This test represented the service limit state of the bridge model, where the applied load is not enough to induce flexural cracks in the model. The second testing scenario included applying a post-cracking service load at the mid-span of each beam. The post-cracking service load level was higher than the cracking load but was not enough to induce a failure in any of the bridge components. The third testing scenario included loading the exterior beam under a four-point loading with the objective of stressing the shear key joint to evaluate it performance. The fourth testing scenario included loading the entire bridge model under four-point loading to evaluate it overall performance and ductility. Finally, the last testing scenario included loading the bridge model to failure to evaluate its strength limit state. The following sections present a detailed discussion for the testing scenarios along with the obtained results and observations.

3.8.1 Service limit state testing

As shown in Figure 3.8-1, the bridge model was provided with seven equally spaced diaphragms. Each diaphragm accommodated two transverse post-tensioning un-bonded CFCC strands with an allowable prestressing force of 60 kip per strand. This transverse post-tensioning system was evaluated during the service limit state testing of the bridge model.

As shown in Figure 3.8-2, a single point load of 15 kip was applied at the mid-span of each beam in the bridge model. The test was executed with three configuration of TPT. First, the service load was applied with a TPT force of 120 kip per diaphragm in all seven diaphragms. Second, the service load was applied with a TPT force of 120 kip in three diaphragms (the two end diaphragms and the middle diaphragm). Third, the service load was applied with no TPT force in any of the diaphragms. In addition, the entire test with various levels of TPT force was repeated using a service load of 30 kip instead of the originally applied force of 15 kip.

Figure 3.8-3 shows the test setup. The load was applied using a 200,000-lb hydraulic cylinder connected to a hydraulic pump. A load cell was provided to monitor the applied load and as shown in Figure 3.8-4, the load was applied first to the exterior beam followed by the interior beam, the intermediate beam, the second interior beam, and finally the second exterior beam. It should be noted that the response of the bridge model when the load was applied on one side was a mirror image to that when the load was applied on the opposite side. To avoid repetition, only the deflection curves obtained from loading one side (exterior, interior, and middle beams) are presented in the discussion.

The response of the bridge model under service loads of 15 kip and 30 kip for different loaded beams and at various levels of TPT force is presented in Figure 3.8-5 through Figure 3.8-7. As shown in these figures, the TPT system does not appear to have any influence of the distribution of the load or the recorded deflection. In addition, no cracks or signs of shear key distress were observed during the test. Therefore, it is reasonable to conclude that TPT force is not mandatory at service limit state and non-prestressed transverse diaphragms along with UHPC shear key joints may be sufficient to distribute the load among the adjacent beams without any crack development.

An effective method of evaluating the response of the bridge model under service loads is to calculate the distribution factors among the beams and compare them for different load levels. The

distribution factor for a beam can be calculated by dividing the deflection of the beam by the sum of deflection of all five beams. Table 3.8-1 and Table 3.8-2 show the deflection and distribution factors under service loads of 15 and 30 kip, respectively.

Figure 3.8-1 Schematic diagram showing the location of the transverse post-tensioning forces

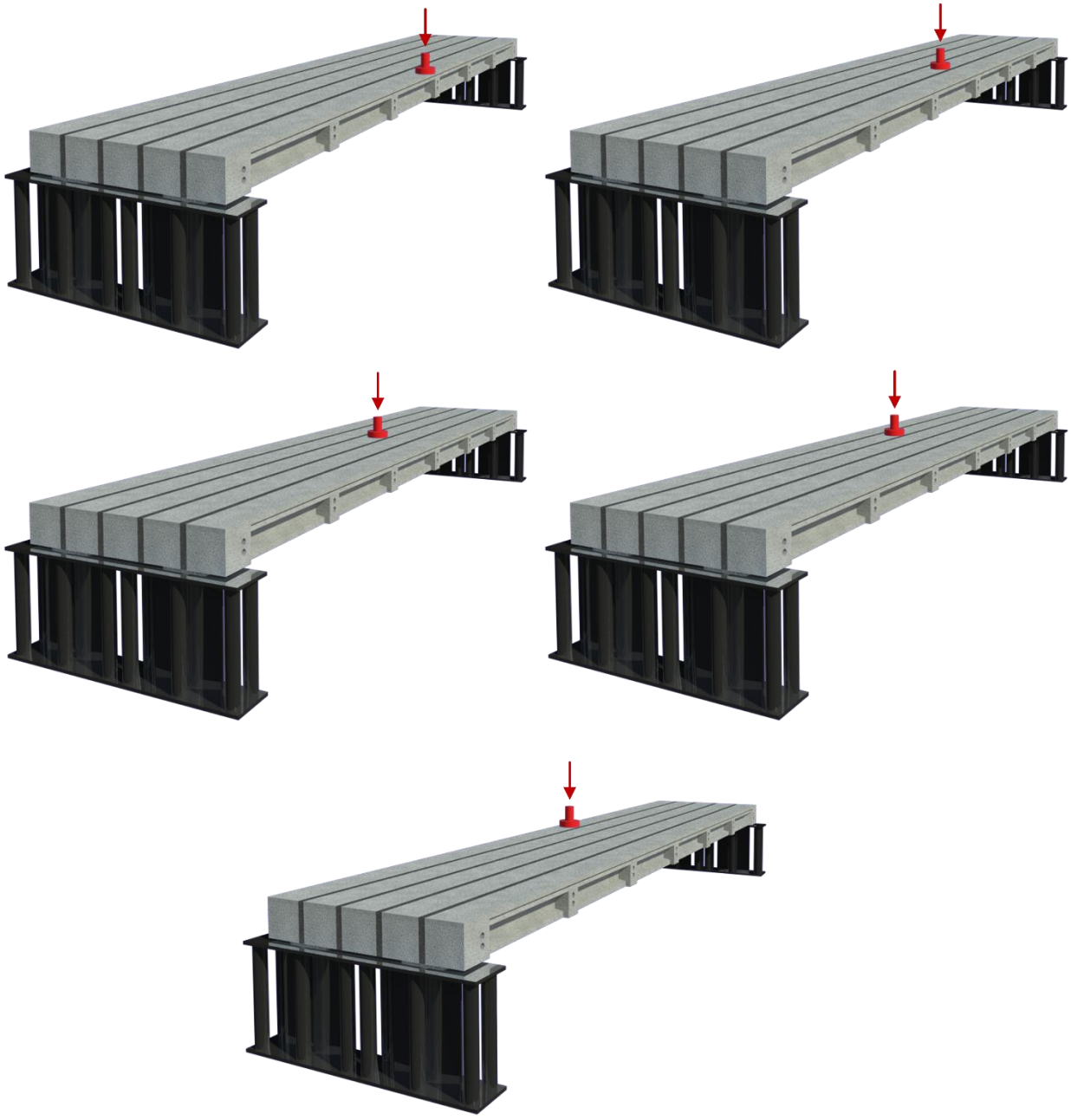

Figure 3.8-2 Sequence of service load application with/without TPT force

Figure 3.8-3 Service limit state testing of the bridge model

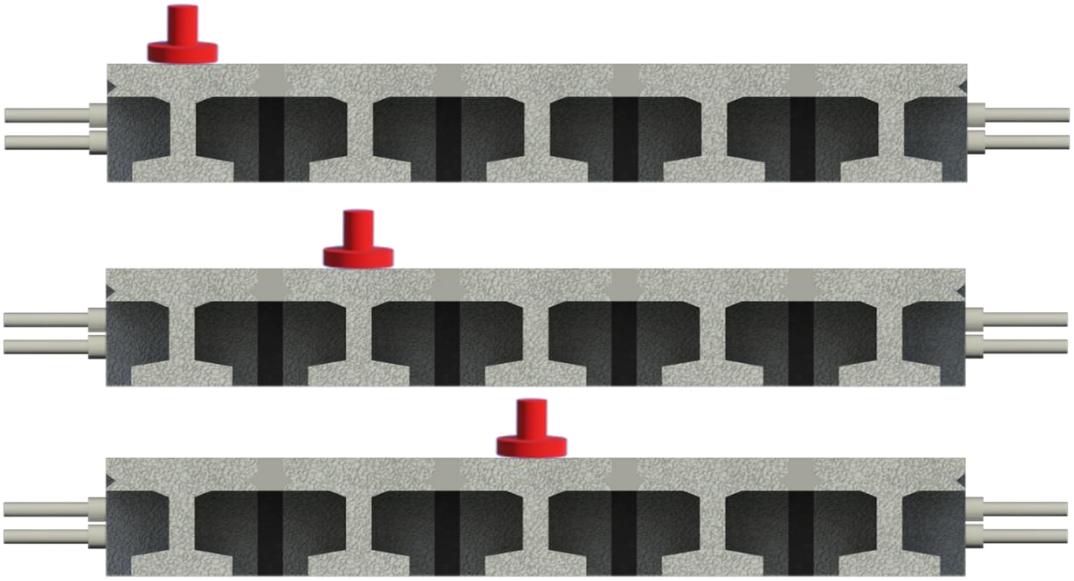

Figure 3.8-4 Sequence of application of service loads in bridge model on: exterior beam, first interior beam, and intermediate beam

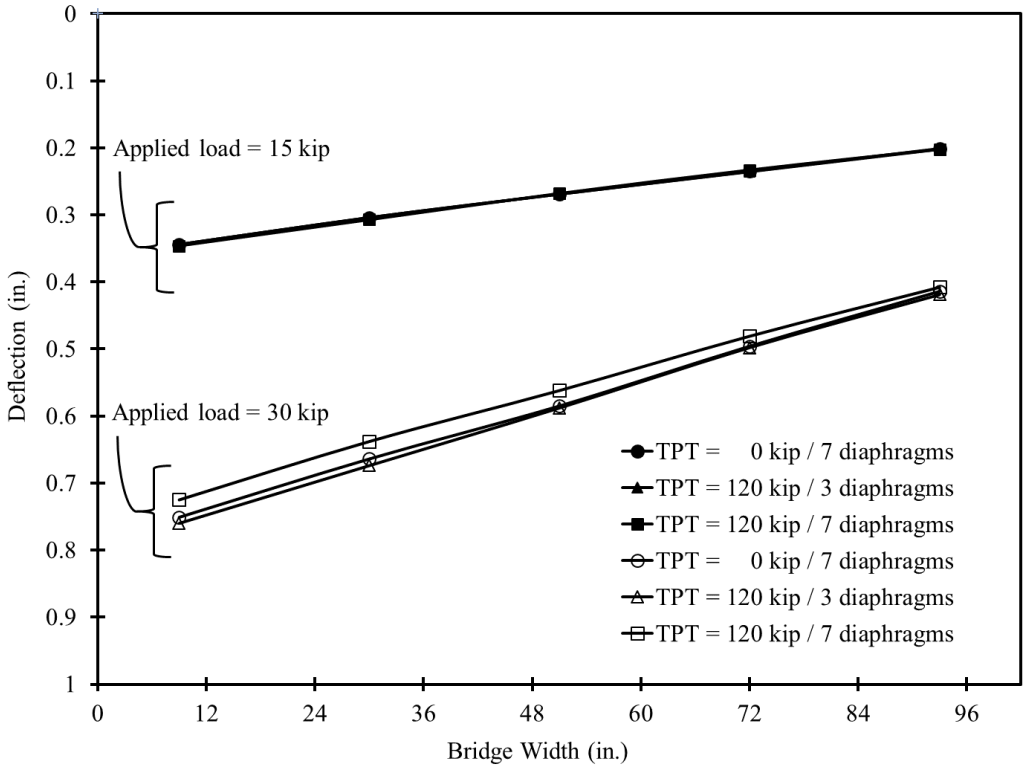

Figure 3.8-5 Deflection curves due to service loads on exterior beam

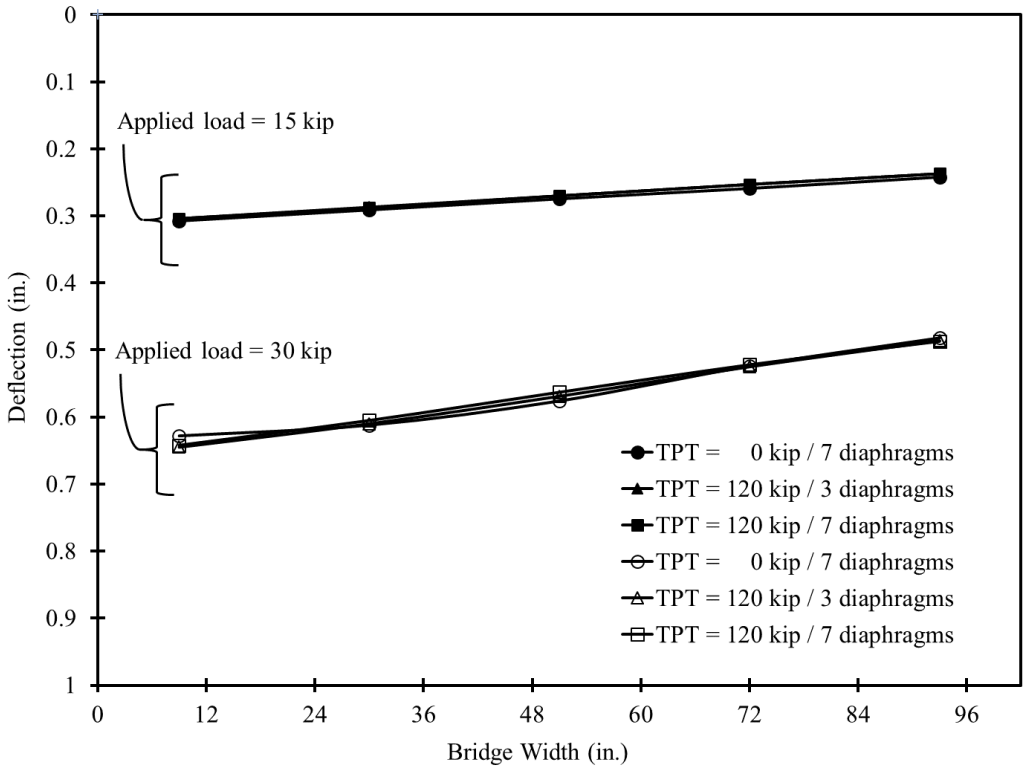

Figure 3.8-6 Deflection curves due to service loads on first interior beam

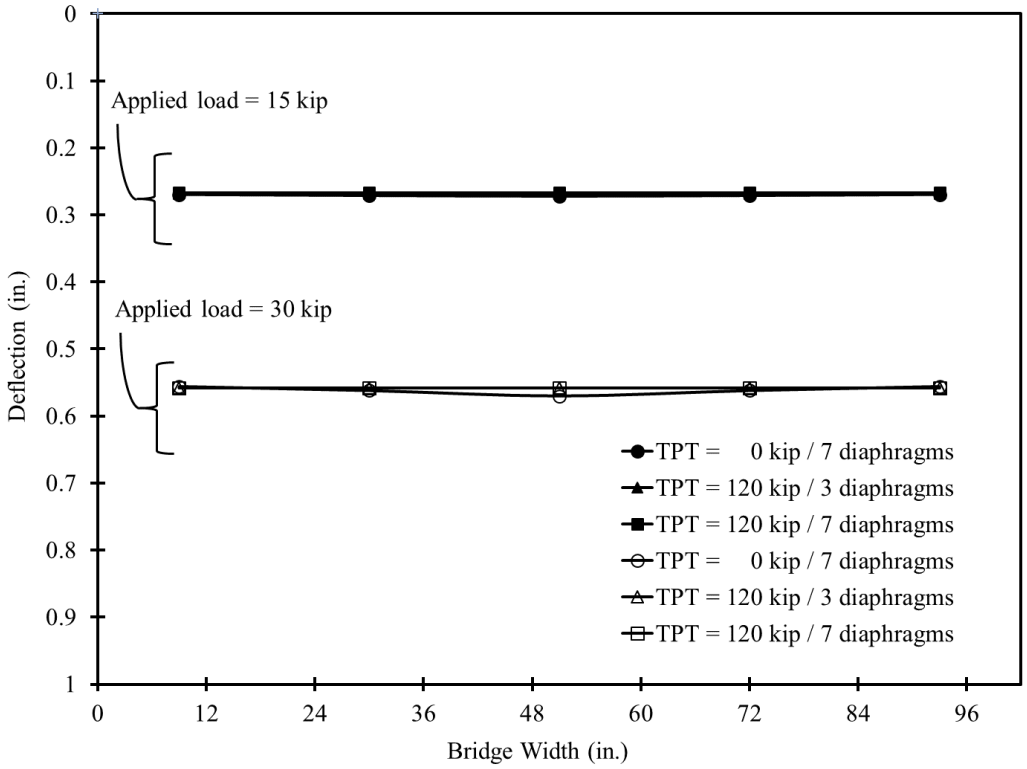

Figure 3.8-7 Deflection curves due to service loads on intermediate beam

Table 3.8-1 Load distribution factors under a point load of 15 kip, no TPT force

	Loaded beam					
	Exterior I beam		Interior I beam		Intermediate beam	
	δ (in.)	D.F.	δ (in.)	D.F.	δ (in.)	D.F.
Exterior I beam	0.344	0.254	0.308	0.224	0.270	0.199
Interior I beam	0.304	0.225	0.291	0.212	0.271	0.200
Intermediate beam	0.269	0.199	0.275	0.200	0.272	0.201
Interior II beam	0.235	0.174	0.259	0.189	0.271	0.200
Exterior II beam	0.201	0.149	0.242	0.176	0.270	0.199

Table 3.8-2 Load distribution factors under a point load of 30 kip, no TPT force

	Loaded beam					
	Exterior I beam		Interior I beam		Intermediate beam	
	δ (in.)	D.F.	δ (in.)	D.F.	δ (in.)	D.F.
Exterior I beam	0.751	0.258	0.628	0.223	0.556	0.198
Interior I beam	0.664	0.228	0.612	0.217	0.562	0.200
Intermediate beam	0.585	0.201	0.576	0.204	0.570	0.203
Interior II beam	0.496	0.170	0.524	0.186	0.562	0.200
Exterior II beam	0.414	0.142	0.482	0.171	0.556	0.198

3.8.2 Post-cracking limit state testing

At the beginning of this state, the bridge model was loaded until flexural cracks developed. Then, a load distribution test using a single point load of 60 kip was performed to evaluate the response of the cracked bridge model. In addition, the exterior beam of the bridge model was loaded under four-point loading without TPT force until signs of shear key distress were recorded. Furthermore, the entire bridge model was loaded under four-point loading to approximately 80% of its ultimate load carrying capacity to evaluate the residual deformation and the absorbed energy near failure.

3.8.2.1 Cracking of bridge model

To induce the flexural cracks, the bridge model was loaded in a four-point loading setup as shown in Figure 3.8-8 and Figure 3.8-9. The distance between the points of load was adjusted to 78 in. The load was applied through cycles of loading and unloading with a load increment of 10 kip between cycles. After each loading cycle, the bridge model was inspected for cracks. The first flexural crack was observed during the 60 kip load cycle (Figure 3.8-10). After evaluating the load-deflection curves, it was determined that the first crack developed at a load level of 53.2 kip with a corresponding deflection of 1.23 in. The development of cracks marked a rapid change in the slope of the load-deflection curve.

Once the first flexural crack developed, a series of strain gages were attached to the soffit of the beams near the crack as shown in Figure 3.8-10. The reading from these strain gages were used later on to evaluate the decompression load of the bridge model and back calculate the effective prestressing force.

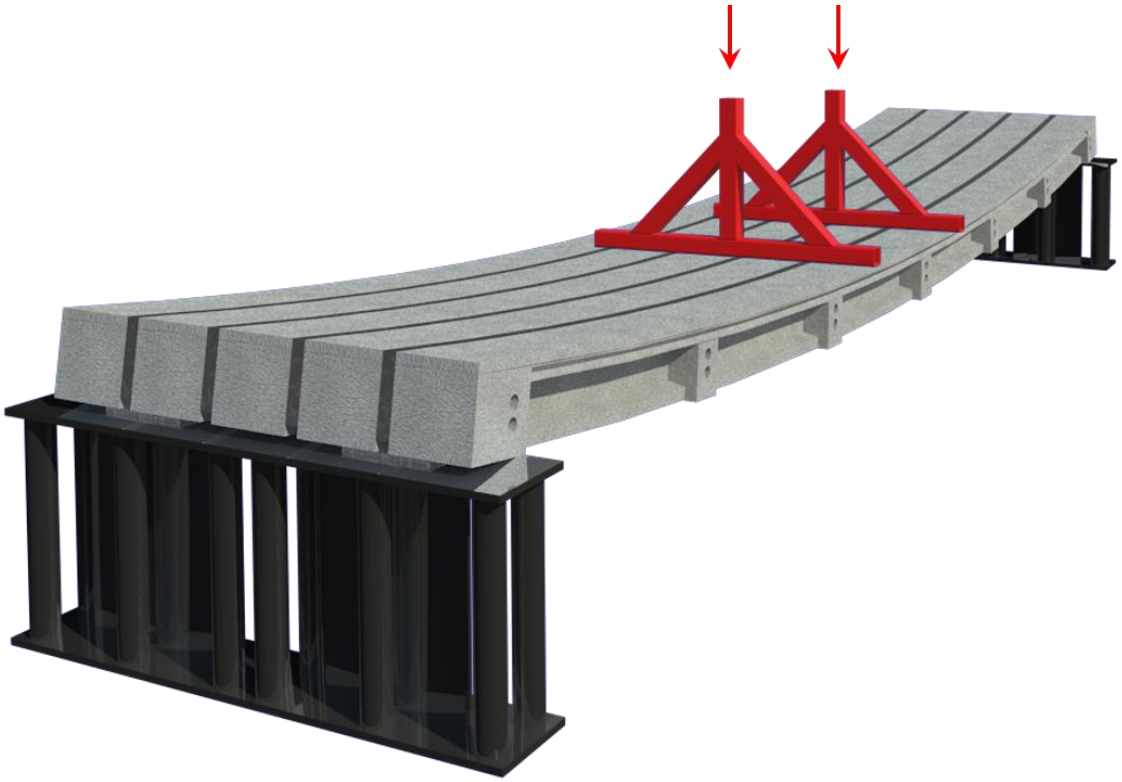

Figure 3.8-8 Four-point-loading setup for inducing flexural cracks

Figure 3.8-9 Four-point loading of bridge model

Figure 3.8-10 Development of first flexural crack in bridge model under four-point loading

3.8.2.2 Load distribution

After cracking the bridge model, the load distribution test was performed again (Figure 3.8-11) with a point load of 60 kip. Based on the results from un-cracked service limit state testing, it was decided to eliminate the TPT force from all the diaphragms.

Similar to the service limit state testing, the deflection of the bridge model was recorded and presented in Figure 3.8-12. As shown in the figure, the deflection curves indicated a uniform load distribution with no observed cracks or shear key distress. In addition, the distribution factors were calculated based on the deflection values as shown in Table 3.8-3 and compared with those obtained from service loads of 15 and 30 kip as shown in Table 3.8-4. As shown in the tables, the distribution factor did not significantly change even when the load increased from 15 to 60 kip. It should be noted that the recorded deflection values at service load of 30 kip are nearly double the values recorded at 15 kip. However, the deflection values at 60 kip is more than double the values at 30 kip. This is due to the cracking and loss of stiffness of the bridge model.

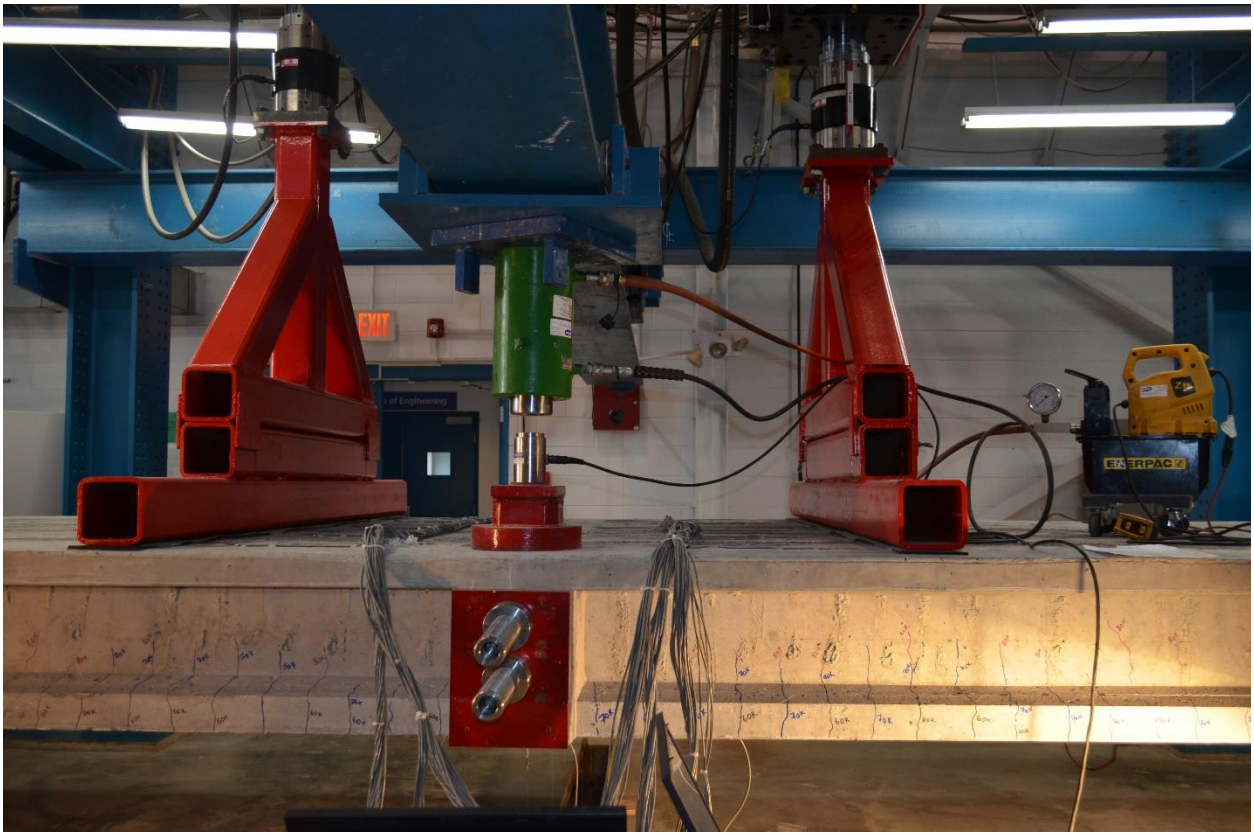

Figure 3.8-11 Post-cracking load distribution test

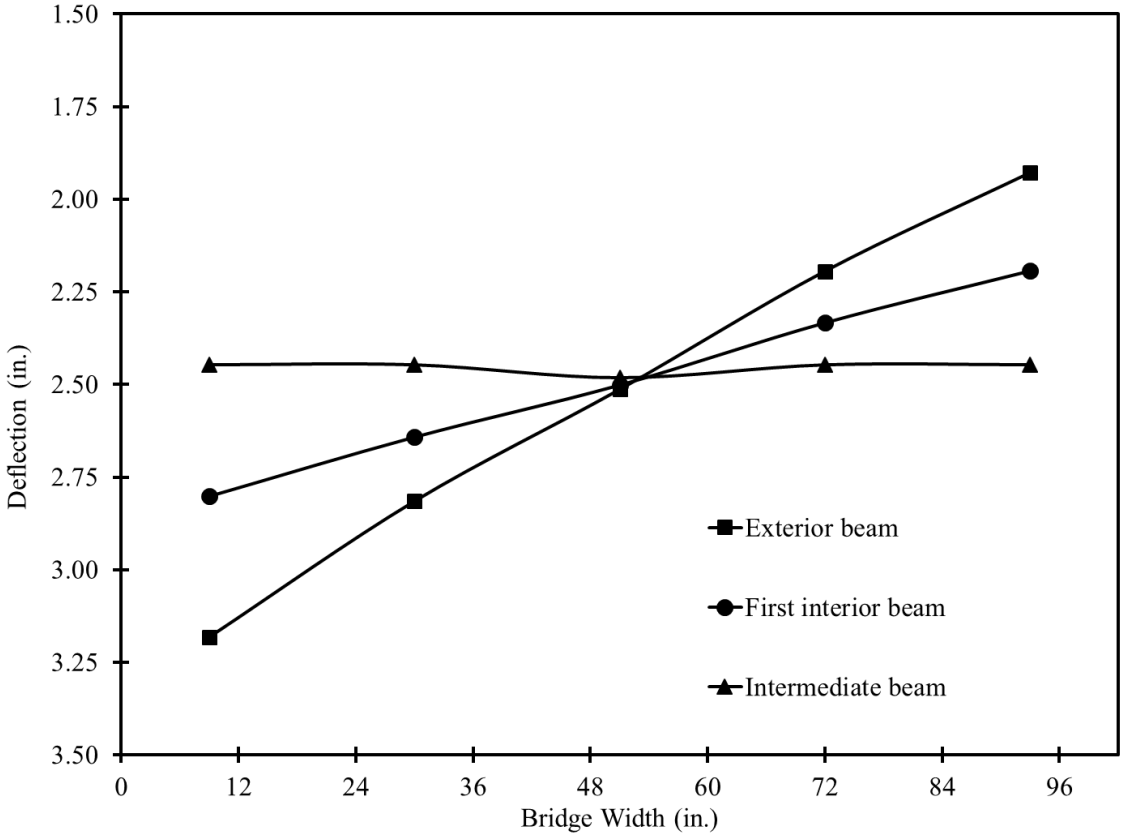

Figure 3.8-12 Deflection curves of bridge model due to post-cracking service load of 60 kip

Table 3.8-3 Load distribution factors under a point load of 60 kip, no TPT force

	Loaded beam					
	Exterior I beam		Interior I beam		Intermediate beam	
	δ (in.)	D.F.	δ (in.)	D.F.	δ (in.)	D.F.
Exterior I beam	3.18	0.251	2.80	0.225	2.45	0.199
Interior I beam	2.81	0.222	2.64	0.212	2.45	0.199
Intermediate beam	2.51	0.199	2.50	0.200	2.48	0.202
Interior II beam	2.19	0.174	2.33	0.187	2.45	0.199
Exterior II beam	1.93	0.153	2.19	0.176	2.45	0.199

Table 3.8-4 Comparison of distribution factors (DF) under point loads of 15, 30, and 60 kip

	Loaded beam								
	Exterior I beam			Interior I beam			Intermediate beam		
	15 kip	30 kip	60 kip	15 kip	30 kip	60 kip	15 kip	30 kip	60 kip
Exterior I beam	0.254	0.258	0.251	0.224	0.223	0.225	0.199	0.198	0.199
Interior I beam	0.225	0.228	0.222	0.212	0.217	0.212	0.200	0.200	0.199
Intermediate beam	0.199	0.201	0.199	0.200	0.204	0.200	0.201	0.203	0.202
Interior II beam	0.174	0.170	0.174	0.189	0.186	0.187	0.200	0.200	0.199
Exterior II beam	0.149	0.142	0.153	0.176	0.171	0.176	0.199	0.198	0.199

3.8.2.3 Shear key testing

The testing scenario was developed to directly evaluate the performance of UHPC shear joints along with the transverse diaphragms. An exterior beam of the bridge model was loaded until localized shear key cracks were developed. As shown in Figure 3.8-13 and Figure 3.8-14, the exterior beam was loaded through a four-point loading setup with 78-in. distance between the two points of load. No TPT force was applied at any of the transverse diaphragms. The load was applied in cycles starting from 60 kip with an increment of 10 kip. The bridge model was inspected for cracks after each load cycle.

No cracks developed at a load level of 70 kip. At a load level of 80 kip, minor cracks developed around the three intermediate diaphragms in addition to a limited hairline crack at the shear key joint near the applied load as shown in Figure 3.8-15 through Figure 3.8-17. All cracks developed on the concrete side of the joint and not on the UHPC side. In addition, when the load increased to 90 kip, the cracks seemed to slightly propagate.

By taking into consideration that failure load of any of the bridge beams was approximately 40.79 kip, it can be concluded that the shear key joint resisted approximately twice the load carrying capacity of a single beam before cracking. In case of interior beam, the load is distributed through two shear key joints instead of one and it is expected that higher resistance would be achieved before cracking the shear key. Since the purpose was not to destroy the shear key joint,

the test was terminated after reaching a load level of 90 kip. Figure 3.8-18 shows the deflection of the bridge model while the load was applied on the exterior beam.

Figure 3.8-13 Schematic diagram showing testing of shear key joint

Figure 3.8-14 Shear key testing of bridge model

Figure 3.8-15 Bottom view of bridge model showing development of cracks at diaphragm

Figure 3.8-16 Localized shear key cracks at load level of 80 kip

Figure 3.8-17 Cracks under a load of 80 kip near intermediate diaphragm

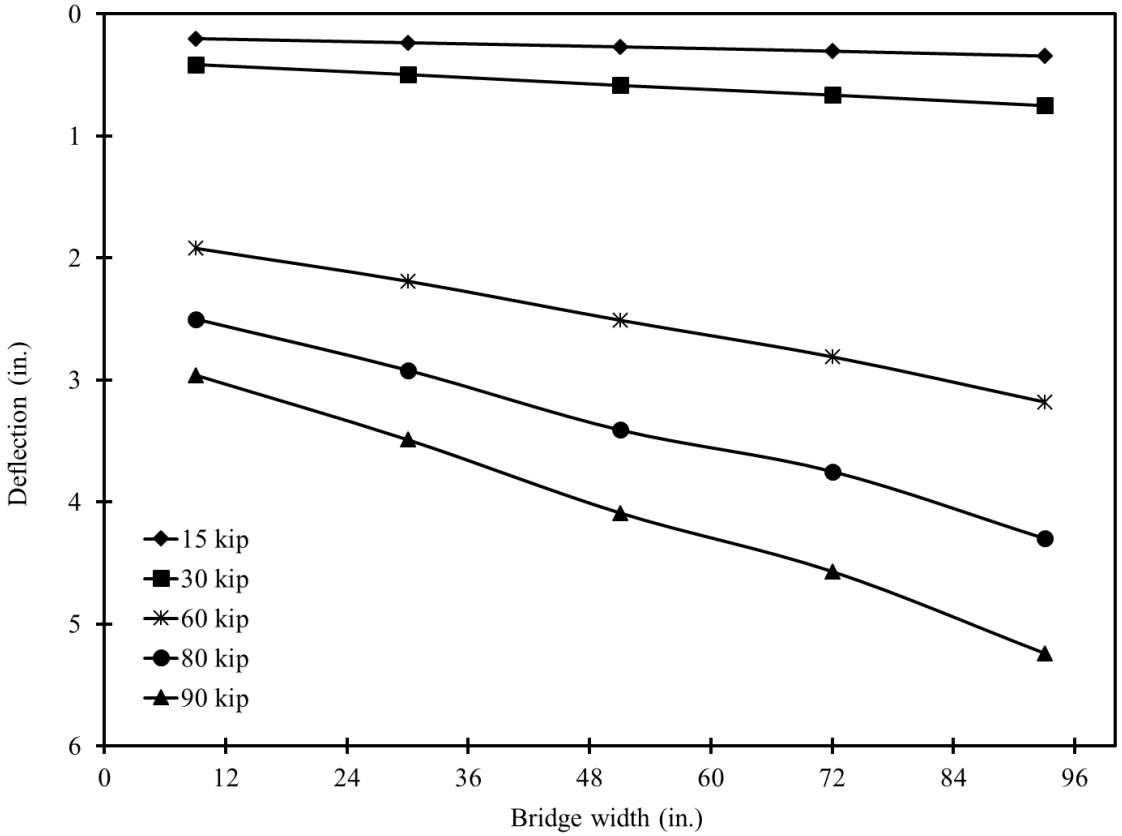

Figure 3.8-18 Deflection curves of bridge model while loading exterior beam

3.8.2.4 Load cycles

After completing the testing scenario for the shear key joint, the test setup was revised back to the four-point loading across the entire width of the bridge model as shown in Figure 3.8-19. At this stage of loading, it was necessary to perform load cycles to separate the elastic energy of the bridge model from the inelastic energy and to determine the decompression load. The loading of the bridge model was applied through cycles of loading and unloading with an increment of 10 kip until a load level of 160 kip. This load level represented approximately 80% of the anticipated ultimate load carrying capacity. The load-deflection curves for all load cycles including those executed while cracking the bridge model are presented in Figure 3.8-20. As shown in the figure, the corresponding deflection for a load of 160 kip was approximately 11.75 in. By the end of the unloading phase, the residual deflection from all loading cycles was approximately 0.95 in.

The decompression load was estimated using the readings from the soffit strain gages and from the load-deflection curves. Figure 3.8-21 shows a typical reading from the soffit strain gage near the crack. As shown in the figure, the strain gage captured positive strain until the flexural crack started to open. With crack opening, the reading from the strain gage did not increase with the load and eventually decreased after further increasing the load. The decompression load can be determined from the maximum strain reading or from the corresponding load that caused the maximum reading.

On the other hand, Figure 3.8-22 shows the method of calculating the decompression load from the load-deflection curves. As shown in the figure, every load-deflection curve had two distinct linear segments. Those segments represented the un-cracked and cracked states of the bridge model. The un-cracked state was achieved when the prestress forced the cracks to close. The cracked state was achieved when the applied load overcame the effect of prestressing and caused the flexural cracks to open. Therefore, the two segments of the curve connected at the decompression load.

The average decompression load from both methods of calculation was approximately 45.97 kip. When back calculating the prestressing force, it was determined that the average prestress loss was approximately 14.8% .

Figure 3.8-19 Load cycle test of bridge model

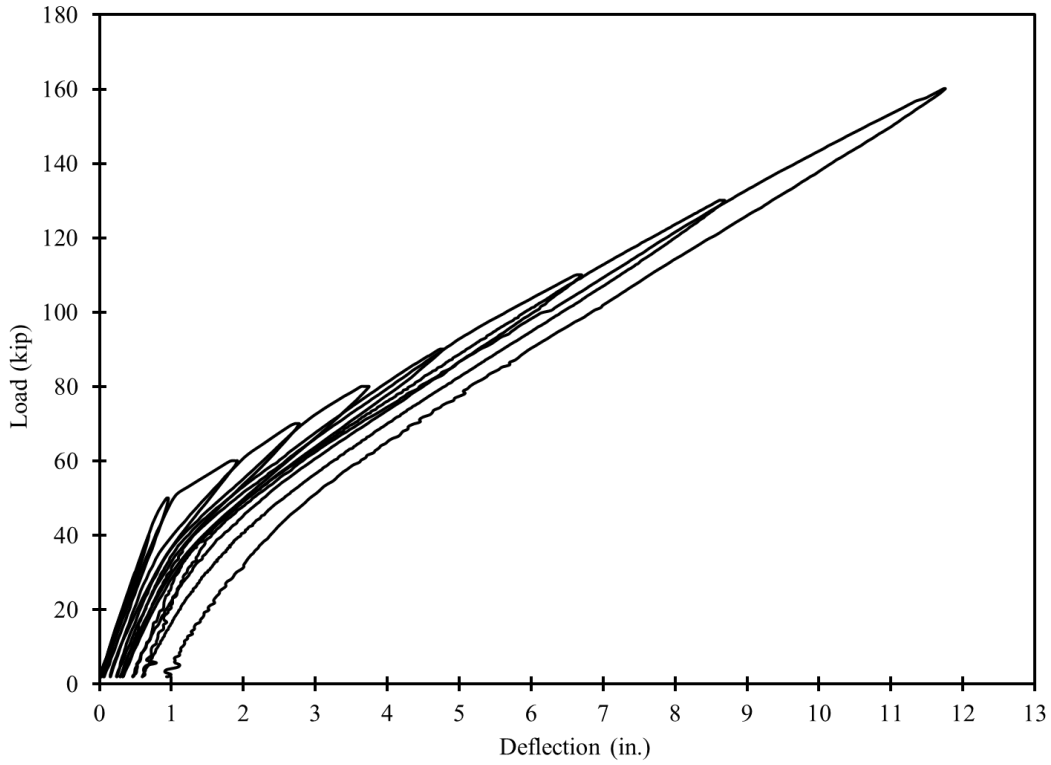

Figure 3.8-20 Load-deflection curves of bridge model under flexural load cycles

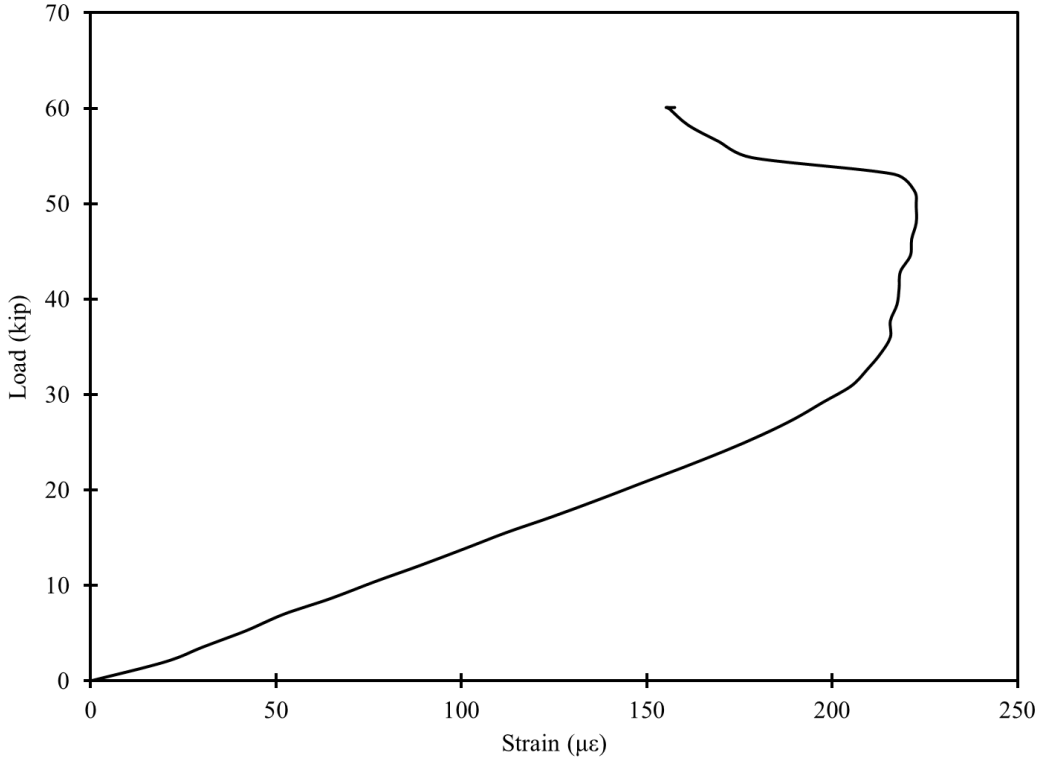

Figure 3.8-21 Load vs. strain at the soffit of the beam after crack initiation

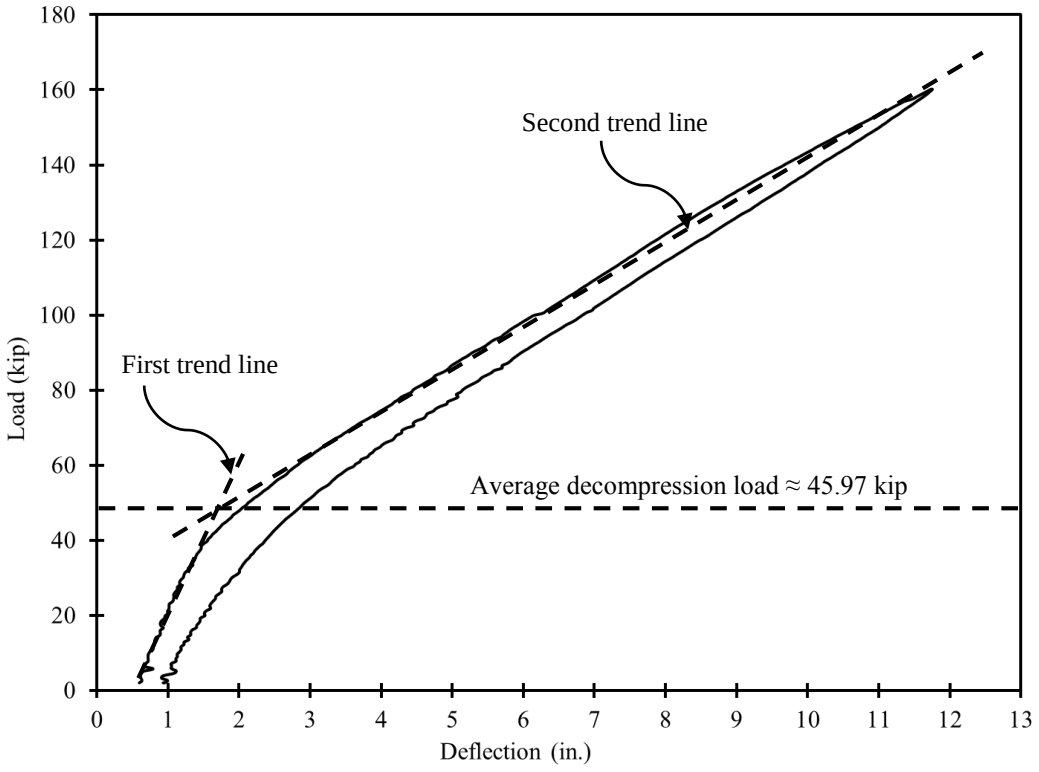

Figure 3.8-22 Estimating decompression load from load-deflection curves

3.8.3 Strength limit state testing

The strength limit state testing of the bridge model included loading the intermediate beam under four-point loading as shown in Figure 3.8-23. The distance between the two points of load was maintained at 78 in. Therefore, no TPT was applied through any of the diaphragms and the TPT strands were removed from the bridge model. One of the main objectives of this test setup was to determinate the efficiency of UHPC shear key joints along with non-prestressed transverse diaphragms on distributing the applied load.

The loading rate was maintained at 4 kip per minute and was applied through two MTS actuators with a maximum capacity of 250 kip, each. The load was applied through a force control module in one continuous phase of loading to failure. Deflection and strain measurements were recorded through a series of LMTs and strain gages, while the load was recorded through two loads cells attached to the actuators. All sensors were connected to the data acquisition system.

The bridge model experienced a significant deflection before failure. As shown in Figure 3.8-24 and Figure 3.8-25, the deflection was noticeable with a naked eye and was accompanied by a dense cracking pattern. The cracks were distributed evenly at a 4.0-in. spacing and was overlapping the location of the stirrups at the mid-third region of the bridge model.

The bridge model achieved a load level of 220 kip with a corresponding deflection of 18.14 in. With further increasing the load, a popping sound corresponding to rupture of CFCC strands was heard. With every strand rupture, spalling of concrete and sudden drop in the load were observed. Initially, the concrete in the top flange did not show any signs of crushing but after the rupture of a few CFCC strands, signs of partial concrete crushing at the exterior beam were observed (Figure 3.8-26 and Figure 3.8-27).

Even with strand rupture, the bridge model continued to support some load at a decreased rate. That was due to the distribution of the load from the intermediate loaded beam to the adjacent beams along with the increased deflection, which allowed a brief relief of the load before the actuators stressed the bridge model again. As shown in Figure 3.8-28 and Figure 3.8-29, the spalling of the concrete and rupture of the CFCC strands took place mainly in the intermediate loaded beam. The adjacent beams were also stressed but to a slightly lesser degree and therefore, they continued to support additional load and did not immediately fail. This observation proved

that the shear key joints and the transverse diaphragm continued to function even after the failure of the intermediate beam.

Through visual inspection, the shear key joints appeared to be in a sound condition until the bridge model reached it maximum load carrying capacity of 220 kip. Based on previous test results, shear key hairline cracks were suspected but it was not possible to check during the loading of the bridge model. After the failure of the intermediate beam, it was visually apparent that the shear key joints next to the intermediate beam were over-stressed with a clear sign of separation and longitudinal cracks at the points of loading. As shown in Figure 3.8-30, equal deflections were recorded under all five beams of the bridge model until the maximum load of 220 kip was reached. After the maximum load, the deflection curve of the loaded beam substantially departed from the rest of the curves of the other beams. This indicated the failure and separation of the loaded beam along with the adjacent shear key joints.

Figure 3.8-31 and Figure 3.8-32 show the load vs. concrete strain and prestressing strain, respectively. Since the beams were constructed with a balanced reinforcement, the strain in the concrete at failure was well within the range of 2,500 to 3,000 με and at the same time the strain in the prestressing strands was within the range of 16,000 με. The strain in the concrete and the prestressing strands in the intermediate beam showed the highest values with the strain in the concrete approximately 3,000 με and the strain in the prestressing strands approximately 16,570 με. The failure however geared toward the tension failure because the added strength in the compression zone by the UHPC shear key joints.

To calculate the ductility ratio of the bridge model, the load deflection curve of the limit state testing was added to those from previous load cycles as shown in Figure 3.8-33 and the area under the curves were calculated and divided into elastic and inelastic zones by estimating the un-loading path from the ultimate load as shown in Figure 3.8-34. Based on the calculations for the areas, the elastic energy was estimated as 2,002.4 kip.in., while the inelastic energy was estimated as 604.4 kip.in. By dividing the inelastic energy by the total energy, the ductility ratio of the bridge model was estimated as 23%. Similar to beams with CFCC reinforcement, the ductility ratio indicated a brittle failure. However, this brittle failure was accompanied by a significant deflection that was enough warning sign that the bridge was over-stressed.

Figure 3.8-23 Four-point loading of intermediate beam at strength limit state testing

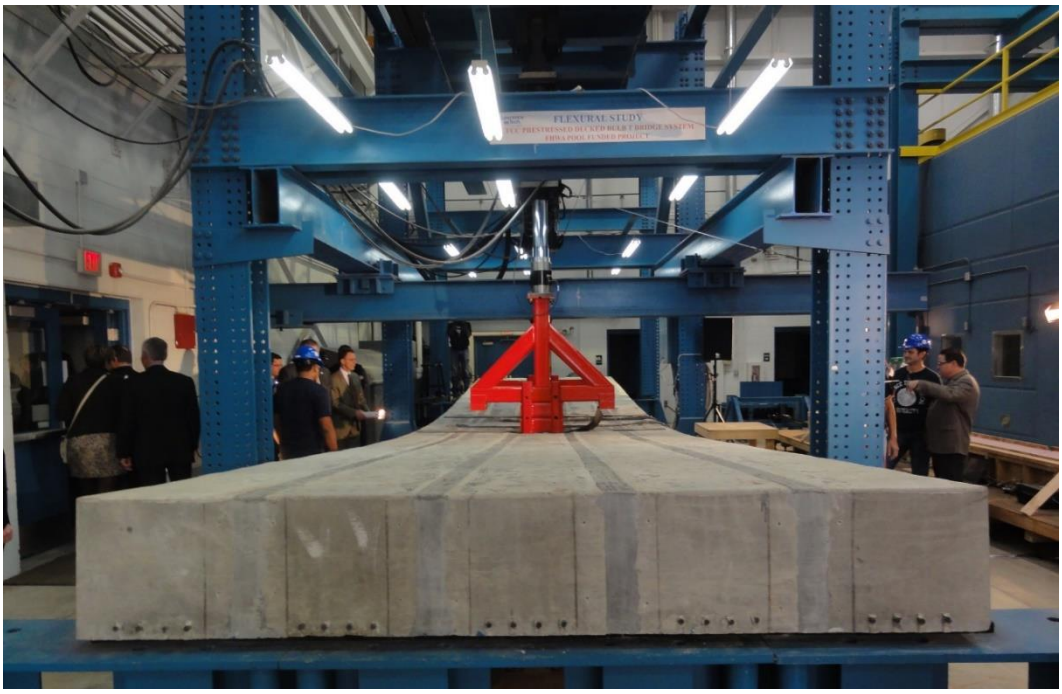

Figure 3.8-24 Deflection of bridge model during strength limit state testing

Figure 3.8-25 Overview of bridge model during strength limit state testing

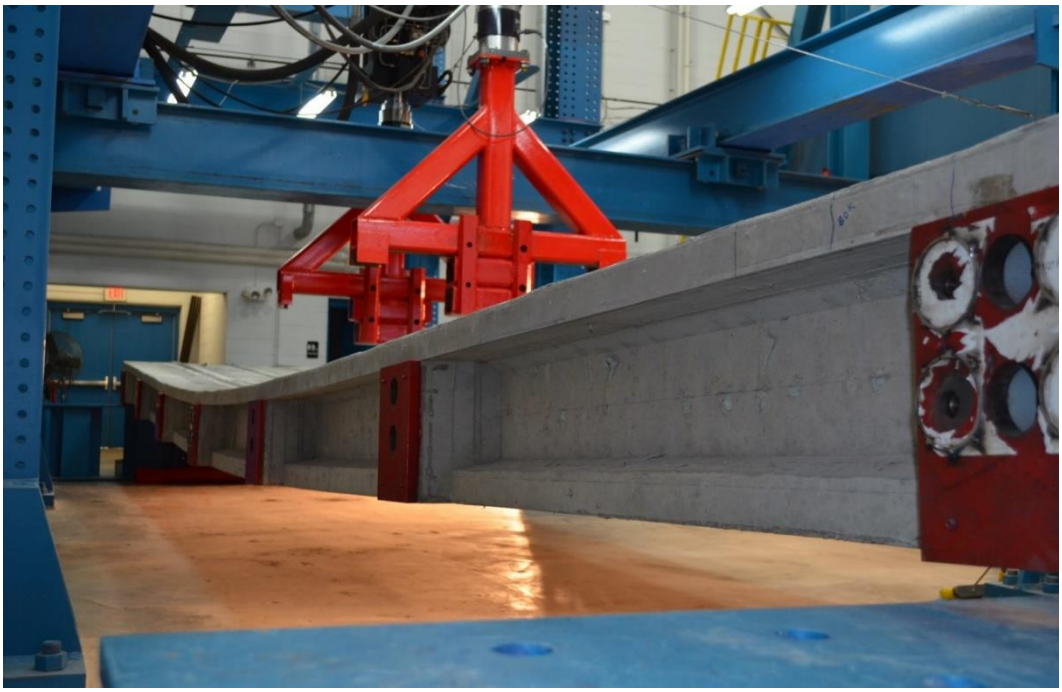

Figure 3.8-26 Bridge model at failure

Figure 3.8-27 Partial concrete crushing in top flange after failure

Figure 3.8-28 Spalling of concrete from bottom of loaded intermediate beam at failure

Figure 3.8-29 Rupture of prestressing CFCC strands in bridge model in intermediate beam

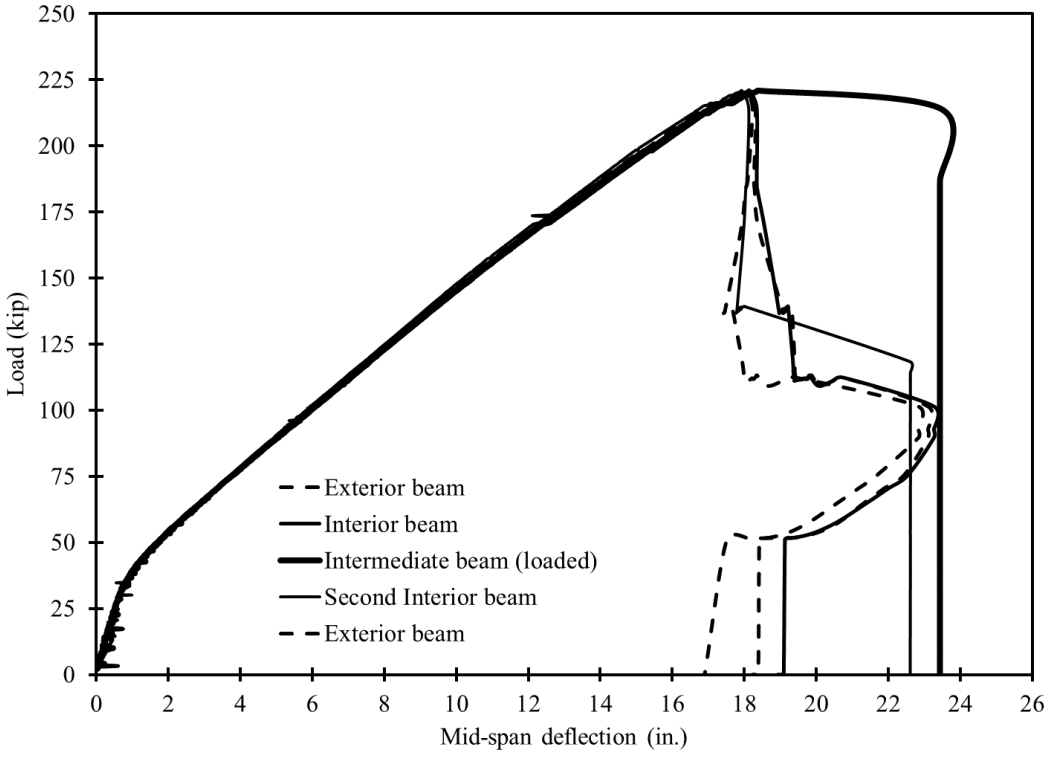

Figure 3.8-30 Load-deflection curves for all beams during ultimate load cycle

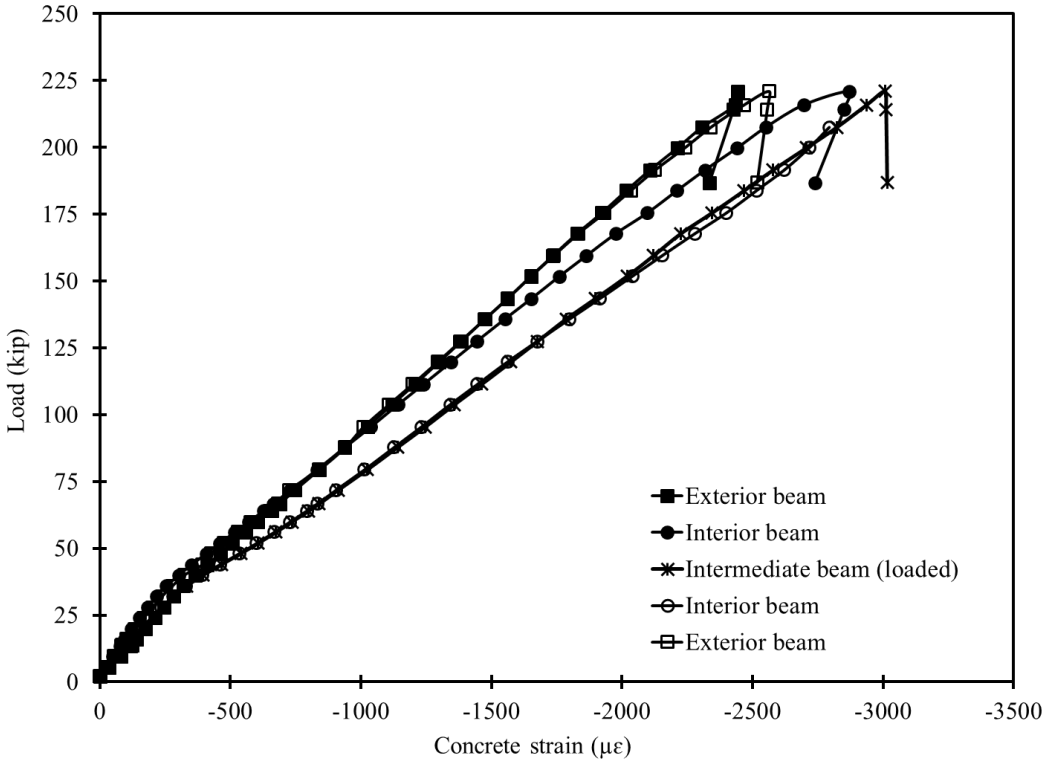

Figure 3.8-31 Load vs. average beam concrete strain during ultimate load cycle

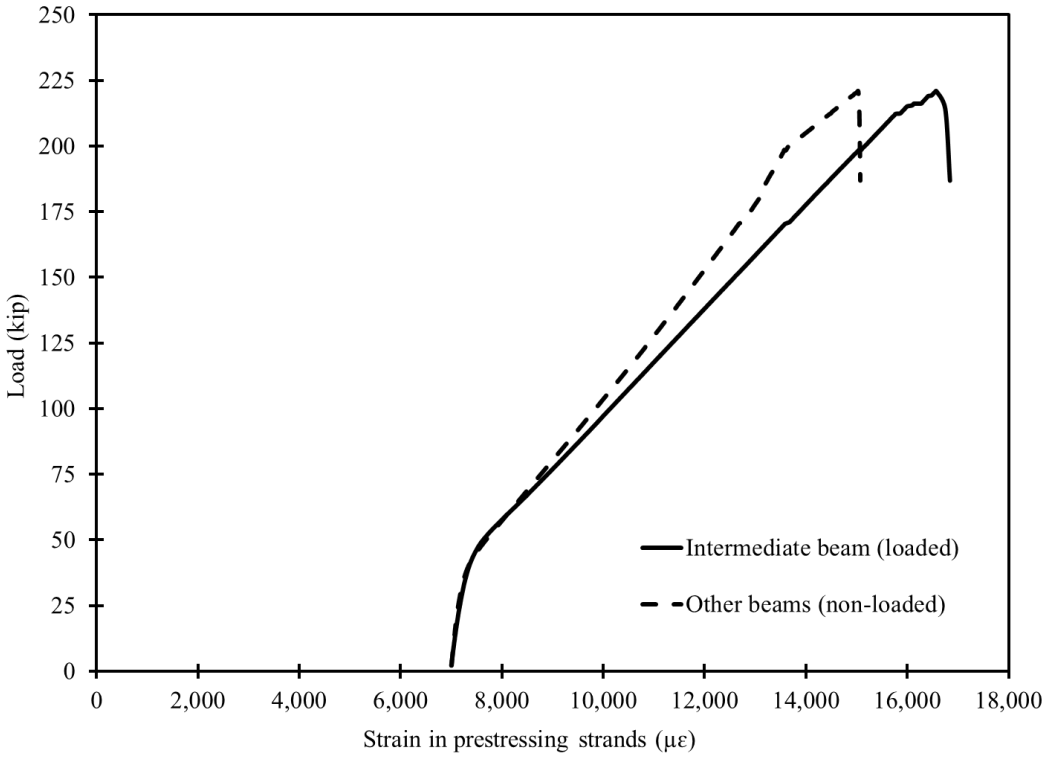

Figure 3.8-32 Load vs. average strain in prestressing strands during ultimate load cycle

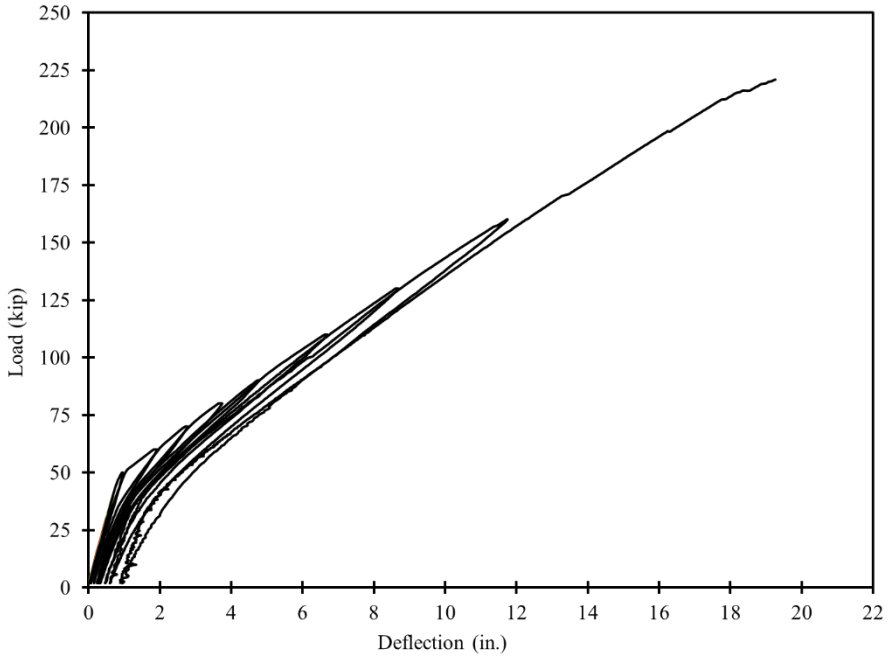

Figure 3.8-33 Combined load-deflection curves for all load cycles to failure of bridge model

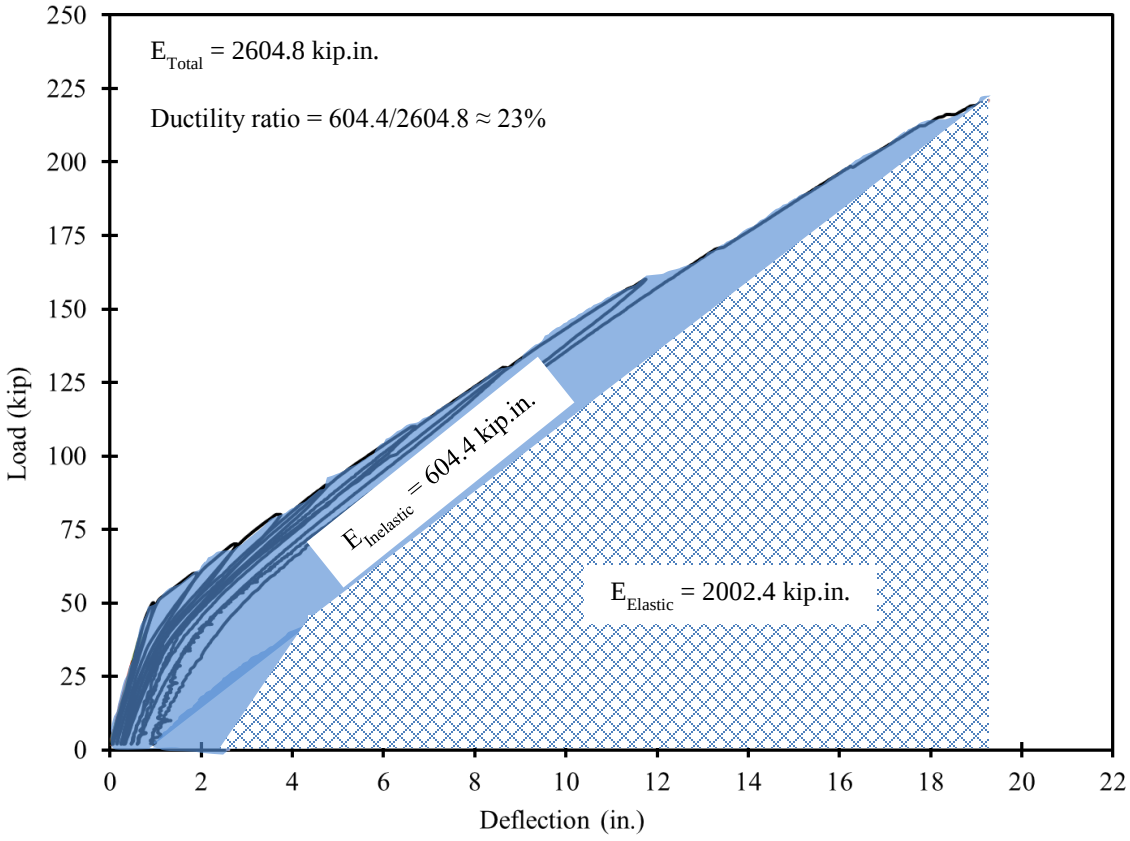

Figure 3.8-34 Ductility ratio of bridge model